Contents

List of Figures

List of Tables

July 6, 2000

Chapter 1

Production, Fragmentation and Spectroscopy

The Tevatron is distiguished from the other current facilities involved in the study of particles containing b-quarks by the size of the cross sections and the range of hadrons containing b-quarks which are produced. The production of b-quarks at the Tevatron and their subsequent fragmentation to a wide range of states is the subject of the present chapter. These processes offer a unique chance to study the dynamics of heavy quark systems in a region where perturbative methods can be applied.

1.1 Open beauty production

1.1.1 The theory of b-quark production†

1.1.1.1 The total cross section

The cross section for the production of a b quark is calculable in perturbative QCD inasmuch as the heavy quark mass, m, is larger than Λ, the scale of the strong interactions. The cross section in the QCD improved parton model is

$$\sigma(S) = \sum_{i,j} \int \frac{dx_1}{x_1}\frac{dx_2}{x_2}\, \hat{\sigma}_{ij}(x_1 x_2 S, m^2, \mu^2) F_i(x_1, \mu^2) F_j(x_2, \mu^2) \ , \tag{1.1}$$

where $\hat{\rho} = 4m^2/\hat{s}, \sigma_0 = \alpha_s^2(\mu^2)/m^2$ and $\hat{s} = x_1 x_2 S$ is the parton total centre-of-mass energy squared. F_i are the momentum densities of the partons in the incoming hadrons. The quantity $\hat{\sigma}_{i,j}$ is the short distance cross section

$$\hat{\sigma}_{i,j}(\hat{s}, m^2, \mu^2) = \sigma_0\ c_{ij}(\hat{\rho}, \mu^2) \ . \tag{1.2}$$

which has a perturbative expansion,

$$c_{ij}(\hat{\rho}, \mu^2/m^2) = c_{ij}^{(0)}(\hat{\rho}) + 4\pi\alpha_s \Big[c_{ij}^{(1)}(\hat{\rho}) + \ln(\frac{\mu^2}{m^2}) \bar{c}_{ij}^{(1)}(\hat{\rho}) \Big] + O(\alpha_s^2) \ . \tag{1.3}$$

The lowest order short distance cross section is calculated from the diagrams in Fig. 1.1. The results for the lowest order total cross sections derived from these diagrams are

†Author: R.K. Ellis

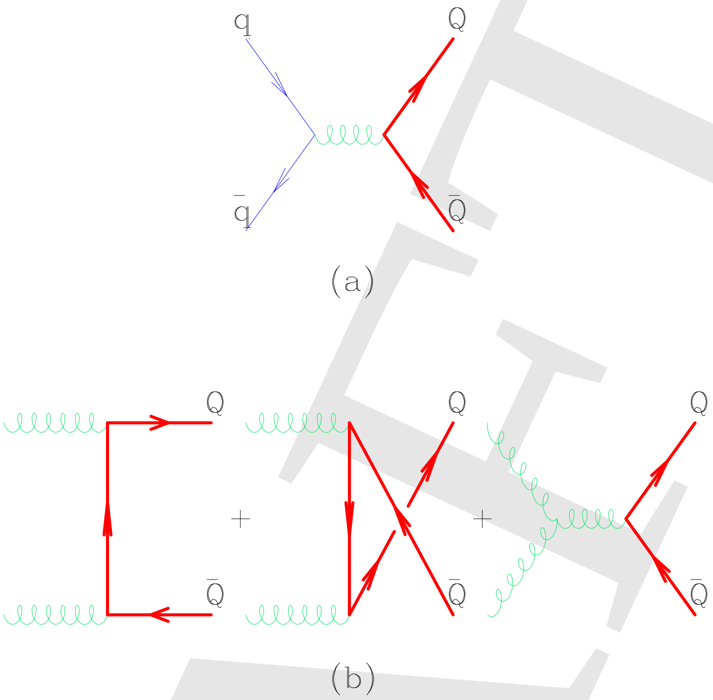

Figure 1.1: Diagrams for heavy quark production in lowest order

$$c^{(0)}_{gg}(\rho) = \frac{\pi\beta\rho}{12}\left\{\frac{3}{N}\Big[(1+\rho-\frac{\rho^2}{2})L(\beta)-1-\rho\Big]+\frac{N}{2V}\Big[3\rho^2L(\beta)-4-5\rho\Big]\right\}$$
$$c^{(0)}_{q\bar{q}}(\rho) = \frac{V}{N^2}\frac{\pi\beta\rho}{24}\Big[2+\rho\Big] \tag{1.4}$$

where $V = N^2-1 = 8, N = 3$ and $\beta = \sqrt{1-\rho}, \rho = 4m^2/s$ and

$$L(\beta) = \frac{1}{\beta}\log\Big[\frac{1+\beta}{1-\beta}\Big] \tag{1.5}$$

The quantities $\bar{c}^{(1)}_{ij}$ and $c^{(1)}_{ij}$ are also known [1], the former analytically and the latter as a numerical fit. The results for these functions as a function of the incoming $\hat{s}$ are shown in Fig. **??**. Two features of $c^{(1)}_{ij}$ as shown in Figs. **??** are worthy of note. The quark-antiquark and gluon-gluon initiated processes have a very rapid rise at threshold.

$$c^{(1)}_{q\bar{q}} \to \frac{c^{(0)}_{q\bar{q}}(\rho)}{8\pi^2}\left[-\frac{\pi^2}{6\beta}+\frac{16}{3}\ln^2(8\beta^2)-\frac{82}{3}\ln(8\beta^2)\right]$$
$$c^{(1)}_{gg} \to \frac{c^{(0)}_{gg}(\rho)}{8\pi^2}\left[\frac{11\pi^2}{42\beta}+12\ln^2(8\beta^2)-\frac{366}{7}\ln(8\beta^2)\right]$$

due to Coulomb $1/\beta$ singularities and to Sudakov double logarithms. Near threshold, these terms give large contributions and require special treatment, such as resummation to all

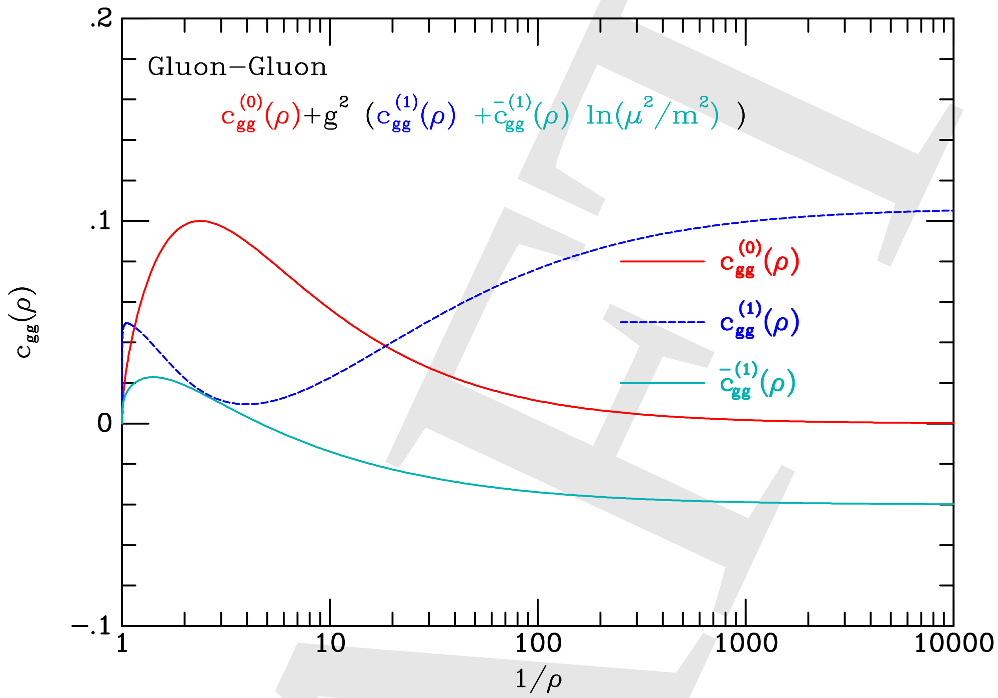

Figure 1.2: The parton level cross section for the gg process

orders. In addition the gg and gq contributions to $c^{(1)}_{ij}$, which involve spin-one gluon exchange in the t-channel, tend to a constant value at large $\hat{s}$. In agreement with the results in Figs. 1.2 and 1.4, the intercept at large s is given by

$$c_{gg} \to 6k \sim 0.1074 \tag{1.6}$$

$$c_{gq} \to \frac{4}{3}k \sim 0.02388 \tag{1.7}$$

where [6]

$$k = \frac{7291}{16200}\frac{1}{8\pi} \approx 0.01791\ . \tag{1.8}$$

The significance of these results for the NLO cross section is shown in Fig. 1.5, illustrating that both the threshold region and the large $\hat{s}$ region are important at NLO.

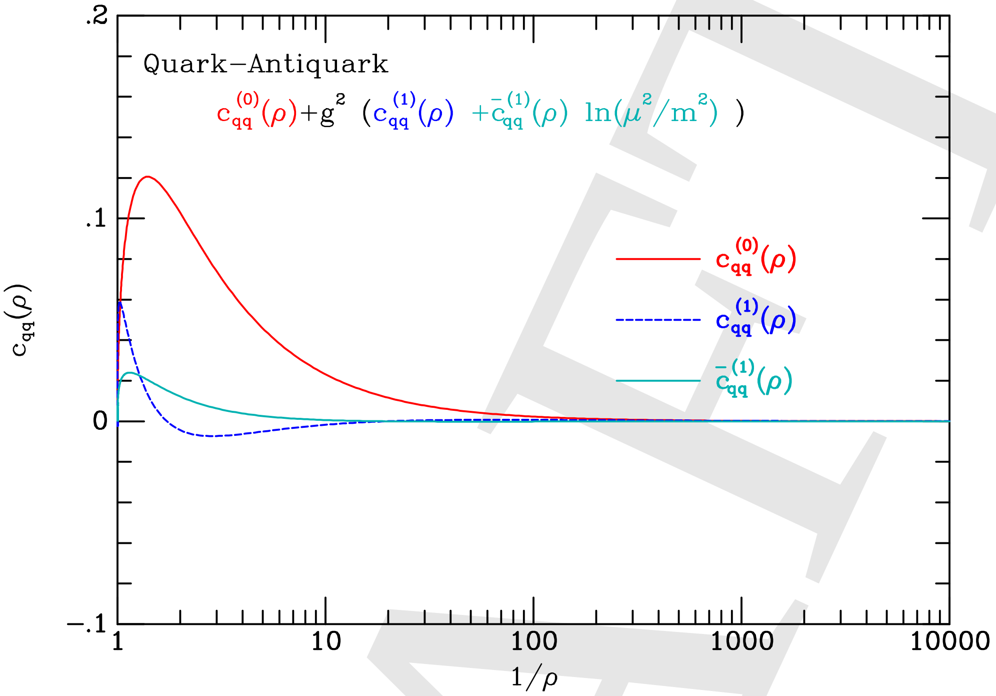

Figure 1.3: The parton level cross section for the $q\bar{q}$ process

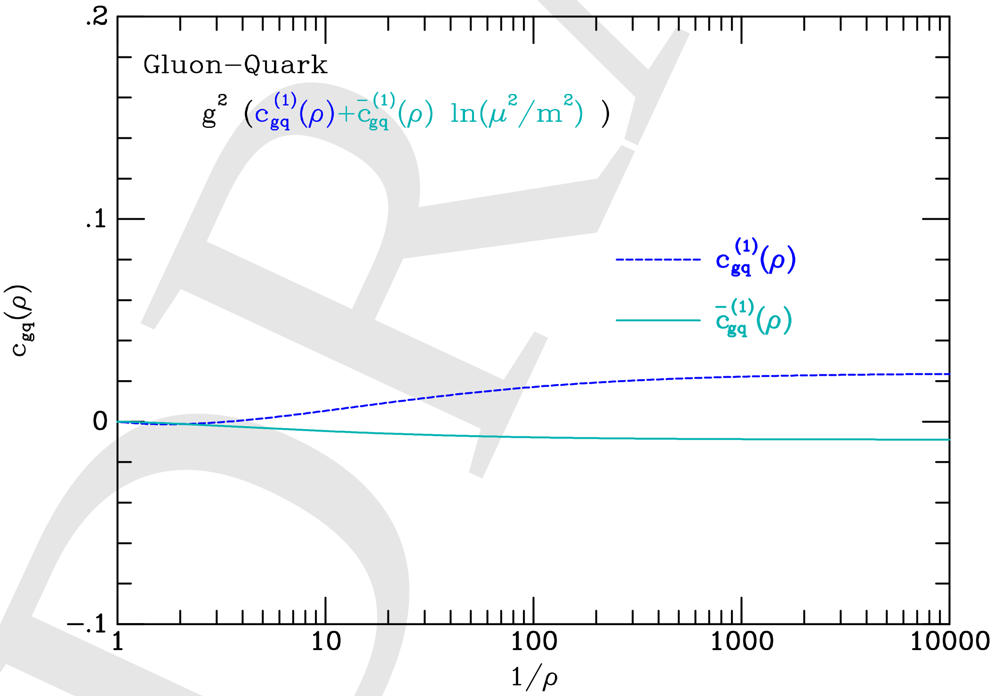

Figure 1.4: The parton level cross section for the gq process

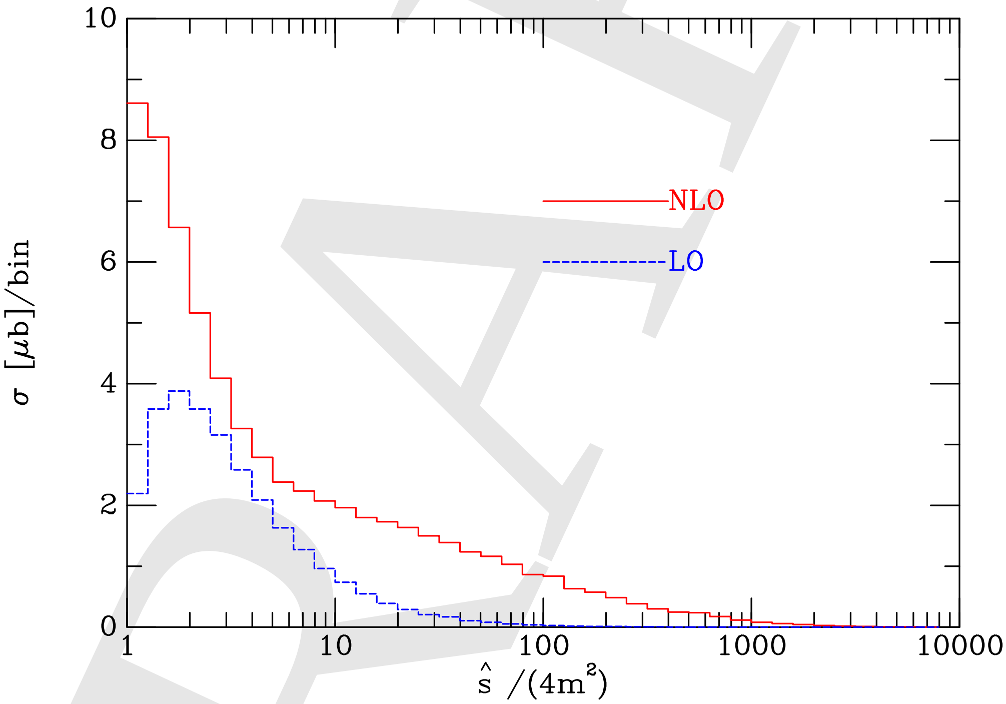

Figure 1.5: Contributions to the total cross section in LO and NLO

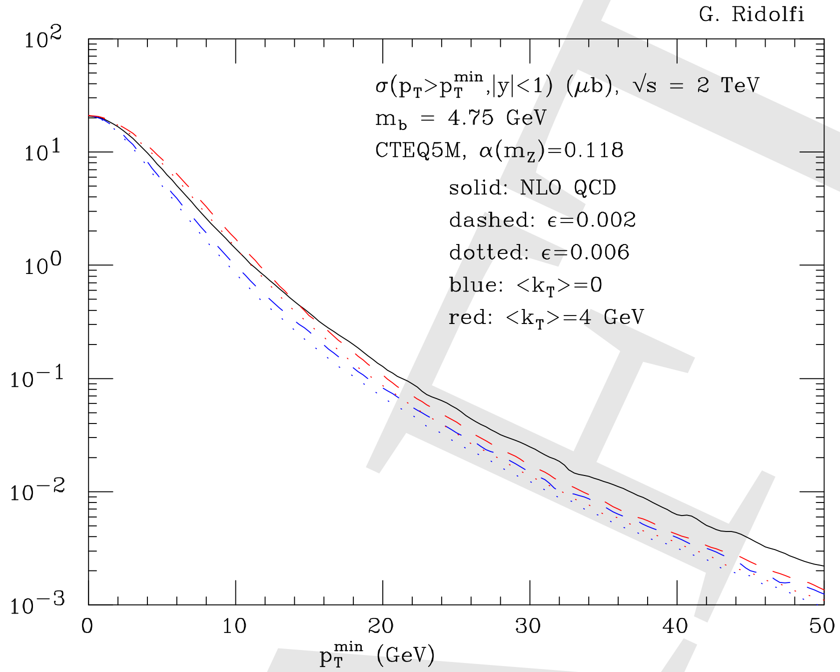

Figure 1.6: xxx

1.1.2 Run II reach for b-quark production

1.1.3 DØ Study of b Jet Production and Run-II Projections †

The differential cross section for b jet production as a function of jet transverse energy is obtained from a sample of muon tagged jets. We discuss b jets as an added tool for understanding b production, and use the present analysis to propose a follow up measurement in Run II. Focus on doubly tagged di(b)jets should significantly reduce both theoretical and experimental uncertainties.

1.1.3.1 Introduction

Previous studies on inclusive b production by the DØ collaboration have concentrated on the b quarks themselves, either as integrated production rates as a function of b quark p_T threshold [13], or the azimuthal correlations between the $b\bar{b}$ pair [14].

In contrast with such studies, we present a somewhat complementary measurement of b production, with the main focus on "b jets" rather than b quarks. "b jets" are defined as hadronic jets carrying b flavor. As such, the object of study is directly an observable, and requires less model dependence when the connection between observation and theory is made.

†Author: Arthur Maciel

This measurement is in straight correspondence with a NLO-QCD calculation by S. Frixione and M. Mangano [15], who highlight the theoretical advantages of considering jets rather than open quarks. For instance, large logarithms that appear at all orders in the open quark calculation (due to hard collinear gluons) are naturally avoided when all fragmentation modes are integrated and it no longer matters what proportion of the jet energy is carried by heavy quarks or by radiation.

Following a brief presentation of our results, we exploit the upgraded capabilities of the run II DØ detector and try to assess what improvements can be expected over the present measurements. Moreover, we consider new experimentation possibilities that might contribute to the ongoing process of understanding the formal description of heavy quark production in the perturbative QCD context.

1.1.3.2 The b Jets Spectrum

This measurement uses 5 pb^{-1} of Run I data from a muon plus jet trigger, from which an inclusive sample of muon tagged jets is extracted. Tagged jets have hadronic E_T above 20 GeV, pseudorapidity $\eta < 0.6$, and carry within their reconstruction cone ($\Delta R = 0.7$) a muon track with p_T above 6 GeV and $\eta < 0.8$. About 36K events are thus selected, and less than 0.5% of them have either a second tagged jet or a doubly tagged one. This is because of the relatively high muon threshold, which also helps to enrich the b flavor content of the sample.

After detection efficiencies and resolution corrections are applied to the inclusive spectrum, the background of light flavors decaying to muons needs to be removed. This is done on a statistical basis, through fits of the distribution of muon transverse momentum with respect to the associated jet axis (P_T^{rel}). We use Monte Carlo templates representing light and heavy quark decay patterns. These templates are floated such as to fit the observed P_T^{rel} spectra in four different transverse energy ranges. Such fits determine the fraction of muons from b decays as a function of tagged jet E_T.

Tagging acceptance corrections are the last step towards a cross section. These stem from the tagging muon threshold, pseudorapidity ranges and the muon-jet association criterion. The unseen lepton energy along the jet also needs to be added (statistically) to the hadronic portion registered in the calorimeter. After such corrections we obtain the b jet differential cross section shown in Fig. 1.7 and defined as the total number of jets carrying one or more b quarks in a given jet E_T bin, and within $\eta < 1$. ($\bar{b}$'s are not counted; technically we count tagging muons of either charge, and divide by twice the inclusive branching ratio of $b \to \mu + X$).

It is observed that this result repeats the general pattern of past b production studies where data lies significantly above the central values of theory prediction, but not incompatibly so, considering the uncertainties on either end.

The measurement uncertainties are driven by the P_T^{rel} fits for the b-fraction, seconded by the tagging acceptance losses, and calorimeter energy scale at lower E_T. A summary of the systematic uncertainties (mostly correlated) in this measurement is shown in Fig. 1.8, and this leads us naturally to a discussion of Run II possibilities.

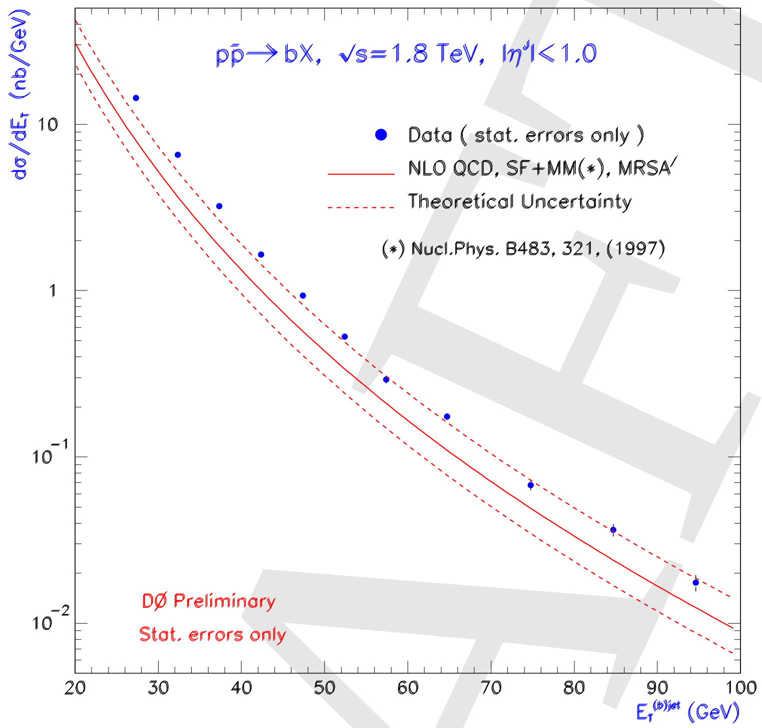

Figure 1.7: The differential b jet cross section and the next to leading order QCD prediction [15]. Data errors shown here are statistical only.

1.1.4 Comments on b Jets for Run II

1.1.4.1 b Tagging

A detector that is fully equipped for b physics should benefit significantly from the study of b jets. The measurement described above is limited in many directions by its tagging method. First in the access to the b-fraction in the inclusive spectrum. The b content of the sample decreases with jet E_T, and the P_T^{rel} fit is no sensitive enough to extract a b signal reliably for jets above 100 GeV. Second, part of the advantage of studying b jets over b quarks is the removal of fragmentation model dependence. This dependence is partially reintroduced when corrections for muon tagging acceptances are performed.

The use of displaced vertex distributions for b tagging not only reduces the b fraction uncertainty to a secondary level in the analysis, but also removes the current upper limit on jet E_T imposed by the P_T^{rel} fits. Some fragmentation model dependence still remains associated with the determination of proper time distributions (decay lengths).

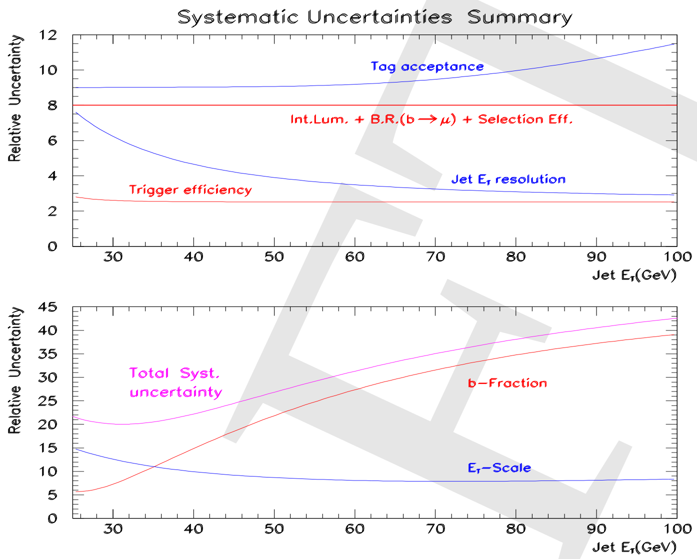

Figure 1.8: A summary of all systematic uncertainties expressed as a relative percentage

1.1.4.2 A Measurement Proposal

One puzzle that arises in the comparison of heavy flavor production data to theory is that alongside some discrepancy in normalization, there is generally fair agreement in angular correlations [14,16,17]. This brings some conflict to the understanding of relative effects between the leading and next to leading order QCD amplitudes. This fact itself, coupled with an interest in b jets, suggests a promising program for Run II.

With an intent on minimizing current uncertainties on both sides, theory and experiment, we can consider a production measurement that is restricted to a limited kinematic regime such as to optimize uncertainties. Consider a cross section for *di-bjets* at wide angles (near back to back), at relatively high E_T and in the central rapidity region.

From the theoretical point of view this experiment favors phase space regions that are further removed from production thresholds, favors high x-values where PDF choices play a much reduced role, and above all, the back to back kinematics suppresses NLO amplitudes in the pQCD calculation (a fact already exploited by CDF in reference [16]).

From the experimental point of view the advantages are many fold. A muon plus jet trigger, very natural to the DØ architecture, (i) enhances the b content of the sample (ii) collects an ideal sample for a second tag by displaced vertex in the non muon side (iii) minimizes the bias towards soft b's inside hard jets because of the imposed muon p_T threshold.

1.1.4.3 Di-bjets with DØ in Run II.

Inspection of Run I DØ data shows that over 70% of the muons in a muon plus jet trigger are naturally associated with a jet. Double tagging (of the b and $\bar{b}$ jets with muon and displaced vertex) naturally yields higher b purity, and largely removes the limitations that are inherent to the P_T^{rel} fits method, in particular the limitation to low E_T because of increasing systematic uncertainties with b jet E_T.

For acceptance projections we can take the present measurement as a starting point, 36K events in 5 pb^{-1} of data. Requirement of a recoil jet (central, opposite hemisphere) also above 20 GeV reduces the sample to 15K muon tagged (p_T above 6 GeV) largely back to back dijet events. With a vertex tagging rate near 10% for the opposite jet we can establish a rule of thumb of 300 events per inverse picobarn.

To access the transverse momentum of the b quark inside the muon tagged jet, we can focus on the tagging muon p_T spectrum (see next section). By applying to our sample the methods used in reference [13] for determining the minimum b quark p_T compatible with our muon and jet thresholds, we find $P_T^{min}(b)$ around 20 GeV.

1.1.4.4 b Quark Production

A natural extension to the run-1 b jets study presented above, is to use the very same data sample and analyze it from the perspective of b quarks rather than b jets. This affords us not only a consistency check against our previous measurements [13,14], but also a chance to significantly extend the reach of their kinematic ranges.

By starting from the data sample described in section 1.1.3.2 we repeat the analysis steps of reference [13] to obtain the integrated b quark production cross section as a function of minimum b quark p_T. Our results are shown in Fig. 1.9 as the higher threshold set of points. In this figure, the present (and preliminary) measurement is confronted with previous results from DØ, CDF (resonant dimuons), and theory [18].

Consistency among all measurements is very satisfactory. As to our new results, besides practically doubling the b p_T threshold reach, perhaps a general trend can now be extracted from Fig. 1.9; that data and theory agreement is improving as one moves towards harder kinematics. Of course this trend could be confirmed with extended and improved measurements in Run II. But the muon inclusive method described in this section has some limitations.

Our uncertainties here are again dominated by systematics rather than statistics. Because the b signal increases with muon p_T, b tagging with P_T^{rel} as a function of muon p_T is more precise than with jet E_T. It is the model dependence, introduced in the access to b quark thresholds as a function of muon acceptance, that completely dominates the uncertainties in this type of measurement.

The full reconstruction of final states into specific B meson production differential cross sections circumvents such uncertainties. CDF [19] has already done so, probing a lower meson p_T region where the data and theory confrontation exhibits the same characteristics

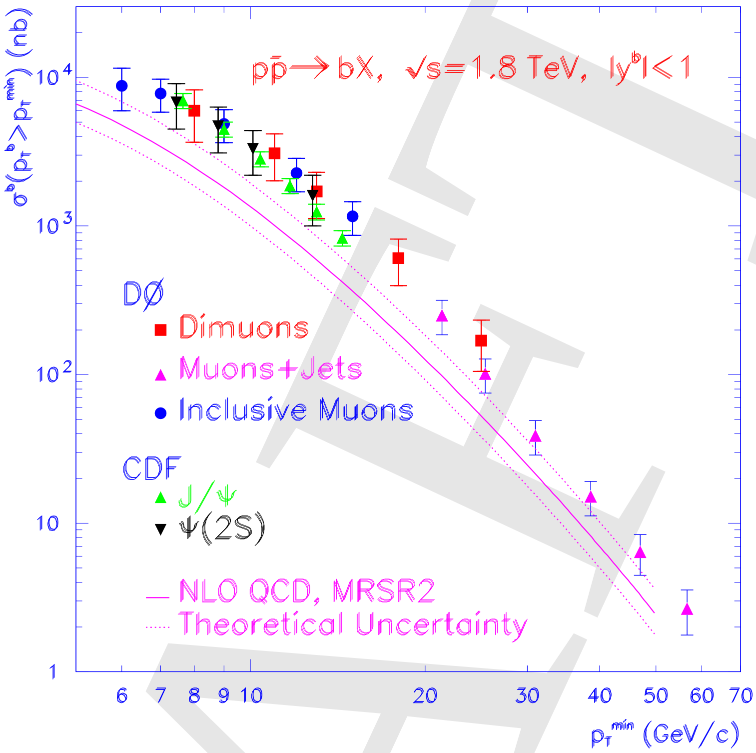

Figure 1.9: [A summary of b production (integrated) cross section measurements.] A summary of b production (integrated) cross section measurements, shown as a function of minimum b quark p_T. The preliminary analysis described here is represented by the higher $P_T^{min}(b)$ triangles.

as the earlier measurements ($P_T^{min}(b) < 30$ GeV) in Fig. 1.9. It would be interesting to inspect whether data and theory converge with increasing meson p_T. Various triggering and offline selection handles exist that could significantly extend meson p_T range. Such studies however lie beyond the scope of the present report.

1.1.4.5 Conclusion

We have presented a Run I cross section measurement for jets carrying b flavor, and have illustrated some of the experimental advantages of studying b jets (which are complementary to b quarks). The b quark cross section extracted from the same data sample confirms previous measurements and significantly extends the b quark p_T reach, while hinting at improved agreement between data and theory as b momentum thresholds increase.

For Run II, a related measurement is envisaged that (i) focuses on dijets (doubly tagged) rather than single jets (ii) restricts the kinematic region of the final states for the sake of optimally reduced uncertainties both in the theoretical and experimental sides.

A muon plus jet(s) trigger is one of the strengths of the DØ experiment, and a center piece for various other physics projects. DØ Run II will for the first time have an internal magnetic volume for precision tracking and vertexing. A muon tagged jets sample is an ideal starting point for the displaced vertex tagging of "other side" jets.

Our brief analysis demonstrates the possibility of a very useful and relatively fast measurement for early run II.

1.2 Quarkonium production

1.2.1 Theory of quarkonium production †

Due to the large mass of the heavy quarks, quarkonia can be approximated in a non-relativistic fashion. This allows quarkonium production to be calculated in a systematic expansion in α_s and in v, the relative velocity of the heavy quarks, using Nonrelativistic QCD (NRQCD) [20,21]. The physical picture of production in NRQCD begins with a hard scattering, in which a $\bar{Q}Q$ pair are produced with any spin, angular and color quantum numbers. This process can be calculated in perturbation theory, with α_s evaluated at a scale $\sim m_b$, $\alpha_s(m_b) \simeq 0.2$. Then the $\bar{Q}Q$ evolve into the final state quarkonium H in some non-perturbative fashion. This is encoded in the NRQCD matrix elements, which due to their non-perturbative nature, are at present extracted from experiment.

The NRQCD factorization formula is the mathematical realization of the above picture. The differential cross section for $A + B \to H + X$ can be written as

$$d\sigma = \sum_{ij} \int dx_1 dx_2 f_{i/A}(x_1) f_{j/B}(x_2) d\hat{\sigma}(ij \to H), \tag{1.9}$$

where the functions $f_{k/C}$ are parton distribution functions, $d\hat{\sigma}(ij \to H)$ is the cross section for producing H by scattering partons i and j, and the sum runs over initial state partons. The partonic cross sections can be written as a product of a short distance process, calculable in a perturbative expansion in α_s, and long distance matrix elements

$$d\hat{\sigma}(ij \to H) = \sum_n C_n^{ij} \langle O^H(n) \rangle. \tag{1.10}$$

**********What is C_n^{ij}?**************. The NRQCD matrix elements scale with a definite power of v, allowing the truncation of the v expansion. For bottomonium, $v_b^2 \sim 1/10$, while for charmonium $v_c^2 \sim 1/4$. So we expect the velocity expansion will work better in the bottom sector than the charm sector.

Using the velocity-scaling and spin-symmetry relations [20,22], the leading matrix elements for direct $\Upsilon(nS)$ production can be reduced to a color-singlet parameter $\langle O_1^{\Upsilon(nS)}(^3S_1) \rangle$ and three color-octet parameters $\langle O_8^{\Upsilon(nS)}(^3S_1) \rangle$, $\langle O_8^{\Upsilon(nS)}(^1S_0) \rangle$, and $\langle O_8^{\Upsilon(nS)}(^3P_0) \rangle$. These matrix elements are enough for a quantitative description of $\Upsilon(nS)$ production. The NRQCD factorization formula (1.10) for direct $\Upsilon(nS)$ production reduces to

†Authors: Eric Braaten, Adam Leibovich

$$d\sigma[\Upsilon(nS)] = d\sigma[b\bar{b}_1(^3S_1)]\langle O_1^{\Upsilon(nS)}(^3S_1)\rangle + d\sigma[b\bar{b}_8(^3S_1)]\langle O_8^{\Upsilon(nS)}(^3S_1)\rangle + d\sigma[b\bar{b}_8(^1S_0)]\langle O_8^{\Upsilon(nS)}(^1S_0)\rangle + \left(\sum_J (2J+1) d\sigma[b\bar{b}_8(^3P_J)]\right)\langle O_8^{\Upsilon(nS)}(^3P_0)\rangle. \quad (1.11)$$

The factor of $2J+1$ in the last term comes from using a spin-symmetry relation to eliminate $\langle O_8^{\Upsilon(nS)}(^3P_J)\rangle$ in favor of $\langle O_8^{\Upsilon(nS)}(^3P_0)\rangle$. Similarly, using velocity-scaling and spin-symmetry, the most important matrix elements for the direct production of the P-wave states $\chi_{bJ}(nP)$, $J=0,1,2$, can be reduced to a color-singlet parameter $\langle O_1^{\chi_{b0}(nP)}(^3P_0)\rangle$ and a single color-octet parameter $\langle O_8^{\chi_{b0}(nP)}(^3S_1)\rangle$. The NRQCD factorization formula (1.10) for direct $\chi_{bJ}(nP)$ production reduces to

$$d\sigma[\chi_{bJ}(nP)] = d\sigma[b\bar{b}_1(^3P_J)]\langle O_1^{\chi_{bJ}(nP)}(^3P_J)\rangle + (2J+1) d\sigma[b\bar{b}_8(^3S_1)]\langle O_8^{\chi_{b0}(nP)}(^3S_1)\rangle. \quad (1.12)$$

In the last term, the factor of $2J+1$ comes from using a spin-symmetry relation to eliminate $\langle O_8^{\chi_{bJ}(nP)}(^3S_1)\rangle$ in favor of $\langle O_8^{\chi_{b0}(nP)}(^3S_1)\rangle$. We can also use a spin-symmetry relation to replace $\langle O_1^{\chi_{bJ}(nP)}(^3P_J)\rangle$ in the first term by $(2J+1)\langle O_1^{\chi_{b0}(nP)}(^3P_0)\rangle$.

The short distance pieces in Eqs. (1.11) and (1.12) are currently known to order α_s^3 [23].[1] The first, non-trivial $p_\perp$ distribution for Υ production starts at order $\alpha_s^3 v^3$, through the color-singlet matrix element $\langle O_1^{\Upsilon(nS)}(^3S_1)\rangle$. The next contribution in the v expansion is order v^7, through the color-octet matrix elements $\langle O_8^{\Upsilon(1S)}(^3S_1)\rangle$, $\langle O_8^{\Upsilon(1S)}(^1S_0)\rangle$, and $\langle O_8^{\Upsilon(1S)}(^3P_J)\rangle$. Since $v^4 \sim 1/100$, it would seem that these contributions should be irrelevant. However, they can be kinematically enhanced. For example, at asymptotically large $p_\perp$, the color-singlet cross section scales as $1/p_\perp^8$.[2] The color-octet $^1S_0$ and ^3P_J cross sections scales as $1/p_\perp^6$, while the color-octet $^3S_1$ cross sections scales as $1/p_\perp^4$. This kinematic enhancement leads to the domination of the fragmentation contribution for the case of ψ production at large transverse momenta. For Υ's, however, most of the data is not in the fragmentation region $p_\perp \gg M_\Upsilon$. Thus, we need to keep the non-fragmentation contributions.

Due to the $p_\perp$ dependence of the cross sections, it is not possible to extract the $^1S_0$ and the ^3P_J color-octet matrix elements independently from the Tevatron data. Instead, only the linear combination

$$M_r^{\Upsilon(nS)} = \langle O_8^{\Upsilon(1S)}(^1S_0)\rangle + \frac{r}{m_b^2}\langle O_8^{\Upsilon(1S)}(^3P_0)\rangle \quad (1.13)$$

can be determined, where for Υ production $r \sim 5$. One way to handle the linear combination is to set one of the matrix elements to 0, and only extract the other. *********Is this comment useful?*********.

By using the vacuum saturation approximation, the color-singlet matrix elements can be related to the wave function or derivatives of the wave function at the origin:

[1] Since $\alpha_s(m_b) \sim 0.2$, the perturbative corrections to the color-singlet and color-octet cross sections may be large. The α_s^4 bremsstrahlung corrections to the differential cross sections have already been calculated [24].

[2] This will change at higher orders in α_s.

$$\langle O_1^{\Upsilon(nS)}(^3S_1)\rangle \simeq \frac{9}{2\pi}|R_{\Upsilon(nS)}(0)|^2, \tag{1.14}$$

$$\langle O_1^{\chi_{bJ}(nP)}(^3P_J)\rangle \simeq (2J+1)\frac{9}{2\pi}|R'_{\chi_{bJ}(nP)}(0)|^2. \tag{1.15}$$

Thus the color-singlet matrix elements can be extracted from Υ decay data or calculated using potential models. Values for these matrix elements are given in Table 1.1.

	$\langle O_1^{\Upsilon(nS)}(^3S_1)\rangle$			$\langle O_1^{\chi_{b0}(nP)}(^3P_0)\rangle$
	phenomenology	potential models		potential models
$\Upsilon(3S)$	4.3 ± 0.9	3.7 ± 1.5	$\chi_b(3P)$	2.7 ± 0.7
$\Upsilon(2S)$	4.5 ± 0.7	5.0 ± 1.8	$\chi_b(2P)$	2.6 ± 0.5
$\Upsilon(1S)$	10.9 ± 1.6	10.8 ± 5.5	$\chi_b(1P)$	2.4 ± 0.4

Table 1.1: Color-singlet matrix elements needed for calculation of Υ and χ_b production in units of GeV^3 for the Υ matrix elements and GeV^5 for the χ_b matrix elements. (From Ref. [25].)

The value of the color-octet matrix elements, however, must be extracted from data. The values of the relevant matrix elements for Υ and χ_b production are shown in Table 1.2 [25]. Feed-down from χ_b's and higher Υ's is important, and must be included when calculating the cross sections and extracting the matrix elements.

The theoretical prediction for the cross section given in Ref. [23] diverges as $p_\perp \to 0$. This divergence is clearly not physical. To correctly handle the low $p_\perp$ region, soft gluon effects must be considered. The resummation of these soft gluons has not been done. One proposal to model the effects of the soft gluons is to give the initial state partons a distribution of transverse momenta [27]. This does regulate the singularity, but introduces model dependence. For the matrix elements in Table 1.2, the extraction only used data with $p_\perp > 8$ GeV to remove the problem of unknown soft gluon emission. Two different parton distribution functions were used for the extraction: MRSTLO and CTEQ5L. The b quark mass used was $m_b = 4.77 \pm 0.11$, where the error due to the mass was included in the error in the table along with the statistical error. There is large uncertainty due to the scale, which can be used as a measure of higher order effects.

Using the matrix elements in Table 1.2, it is possible to predict the differential cross section for Υ production at the Tevatron. In Fig. 1.10, we show the differential cross section for $\Upsilon(1S)$ production at the Run II of the Tevatron. The rate is based on a rapidity range $|y| \leq 0.4$.

Similarly, in Fig. 1.11 we show the differential cross section for $\Upsilon(2S)$ production at Run II, and in Fig. 1.12 is the prediction at Run II for $\Upsilon(3S)$.

The rate at low $p_\perp$ should not be taken seriously in any of these plots, since soft gluon effects have not been taken into account, as mentioned earlier. The predicted cross sections are slightly larger ($\sim 20\%$) than the cross sections at CDF Run I, due to the larger center of mass energy, as shown in Fig. 1.13 where the percentage increase in cross section at Run

	CTEQ5L		MRSTLO	
$\langle O_8(^3S_1)\rangle^{\Upsilon(3S)}$	3.6 ± 1.9	3.9 ± 1.7	3.7 ± 2.1	4.1 ± 1.9
$\langle O_8(^1S_0)\rangle^{\Upsilon(3S)}$	5.4 ± 4.3	0	7.5 ± 4.9	0
$\frac{5}{m_b^2}\langle O_8(^3P_0)\rangle^{\Upsilon(3S)}$	0	5.7 ± 4.6	0	7.9 ± 5.2
$\langle O_8^{\chi_{b0}(2P)}(^3S_1)\rangle$	0.8 ± 1.1		1.2 ± 1.3	
$\langle O_8^{\Upsilon(2S)}(^3S_1)\rangle$	16.4 ± 5.7	15.6 ± 5.2	17.4 ± 6.4	16.8 ± 5.8
$\langle O_8^{\Upsilon(2S)}(^1S_0)\rangle$	-10.8 ± 9.7	0	-9.5 ± 11.1	0
$\frac{5}{m_b^2}\langle O_8^{\Upsilon(2S)}(^3P_0)\rangle$	0	-11.2 ± 10.2	0	-9.7 ± 11.6
$\langle O_8^{\chi_{b0}(1P)}(^3S_1)\rangle$	1.5 ± 1.1		1.9 ± 1.3	
$\langle O_8^{\Upsilon(1S)}(^3S_1)\rangle$	2.0 ± 4.1	3.0 ± 3.8	0.4 ± 4.7	1.8 ± 4.4
$\langle O_8^{\Upsilon(1S)}(^1S_0)\rangle$	13.6 ± 6.8	0	20.2 ± 7.8	0
$\frac{5}{m_b^2}\langle O_8^{\Upsilon(1S)}(^3P_0)\rangle$	0	13.9 ± 7.1	0	20.7 ± 8.1

Table 1.2: Color-octet matrix elements needed for calculation of Υ and χ_b production in units of 10^{-2} GeV^3. Only data with $p_\perp > 8$ GeV was used in the extraction. The error bars are statistical errors only. (From Ref. [25].)

II is shown. The solid line is for $\Upsilon(1S)$, dotted for $\Upsilon(2S)$, and dashed for $\Upsilon(3S)$ (hidden behind the solid curve).

Spin symmetry relates η_b and h_b matrix elements to those for Υ and χ_b:

$$\langle O_1^{\eta_b(nS)}(^1S_0)\rangle = \frac{1}{3}\langle O_1^{\Upsilon(nS)}(^3S_1)\rangle[1 + O(v^2)], \tag{1.16}$$

$$\langle O_8^{\eta_b(nS)}(^1S_0)\rangle = \frac{1}{3}\langle O_8^{\Upsilon(nS)}(^3S_1)\rangle[1 + O(v^2)], \tag{1.17}$$

$$\langle O_8^{\eta_b(nS)}(^3S_1)\rangle = \frac{1}{3}\langle O_8^{\Upsilon(nS)}(^1S_0)\rangle[1 + O(v^2)], \tag{1.18}$$

$$\langle O_8^{\eta_b(nS)}(^1P_1)\rangle = \frac{1}{3}\langle O_8^{\Upsilon(nS)}(^3P_0)\rangle[1 + O(v^2)], \tag{1.19}$$

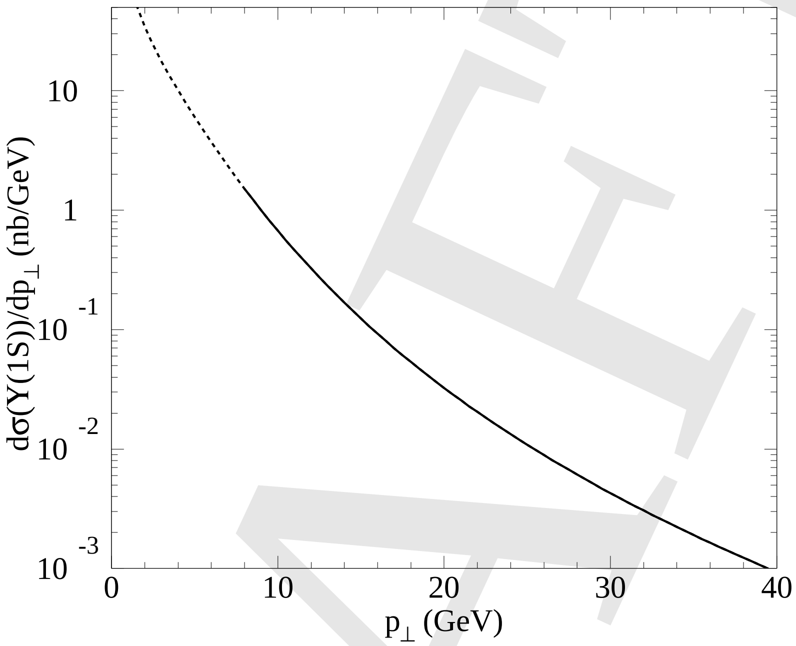

Figure 1.10: Differential cross section for $\Upsilon(1S)$ production at Run II. The rate is based on a rapidity range of $|y| \leq 0.4$.

$$\langle O_1^{h_b(nP)}(^1P_1)\rangle = 3\langle O_1^{\chi_{b0}(nP)}(^3P_0)\rangle[1+O(v^2)], \tag{1.20}$$
$$\langle O_8^{h_b(nP)}(^1S_0)\rangle = 3\langle O_8^{\chi_{b0}(nP)}(^3S_1)\rangle[1+O(v^2)]. \tag{1.21}$$

Therefore it is possible to make a prediction for the rates of these particles at Run II:

$$\begin{aligned} d\sigma[\eta_b(nS)] &= d\sigma[b\bar{b}_1(^1S_0)]\langle O_1^{\eta_b(nS)}(^1S_0)\rangle + d\sigma[b\bar{b}_8(^1S_0)]\langle O_8^{\eta_b(nS)}(^1S_0)\rangle \\ &\quad + d\sigma[b\bar{b}_8(^3S_1)]\langle O_8^{\eta_b(nS)}(^3S_1)\rangle + d\sigma[b\bar{b}_8(^1P_1)]\langle O_8^{\eta_b(nS)}(^1P_1)\rangle \\ &= d\sigma[b\bar{b}_1(^1S_0)]\langle O_1^{\eta_b(nS)}(^1S_0)\rangle + \frac{1}{3}d\sigma[b\bar{b}_8(^1S_0)]\langle O_8^{\Upsilon(nS)}(^3S_1)\rangle \\ &\quad + \frac{1}{3}d\sigma[b\bar{b}_8(^3S_1)]\langle O_8^{\Upsilon(nS)}(^1S_0)\rangle + \frac{1}{3}d\sigma[b\bar{b}_8(^1P_1)]\langle O_8^{\Upsilon(nS)}(^3P_0)\rangle, \end{aligned} \tag{1.22}$$

and

$$\begin{aligned} d\sigma[h_b(nP)] &= d\sigma[b\bar{b}_1(^1P_1)]\langle O_1^{h_b(nP)}(^1P_1)\rangle + d\sigma[b\bar{b}_8(^1S_0)]\langle O_8^{h_b(nP)}(^1S_0)\rangle \\ &= d\sigma[b\bar{b}_1(^1P_1)]\langle O_1^{h_b(nP)}(^1P_1)\rangle + 3d\sigma[b\bar{b}_8(^1S_0)]\langle O_8^{\chi_b(nP)}(^3S_1)\rangle. \end{aligned} \tag{1.23}$$

Since we do not know the branching ratios for η_b or h_b, it is not possible to predict the full production rates without introducing model dependence. Instead we show only the

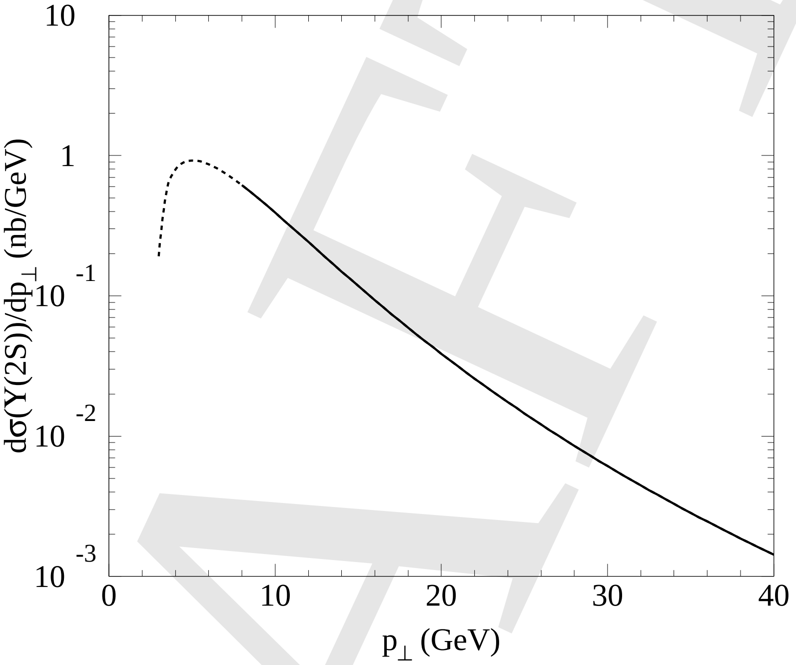

Figure 1.11: Differential cross section for $\Upsilon(2S)$ production at Run II. The rate is based on a rapidity range of $|y| \leq 0.4$.

direct $\eta_b(1S)$ and $h_b(1P)$ rate as examples. We also do not know the individual $\langle O_8^{\Upsilon}(^1S_0)\rangle$ and $\langle O_8^{\Upsilon}(^3P_0)\rangle$ matrix elements, needed for the η_b cross section. The rate is dominated by the color-singlet piece, so this does not lead to a large uncertainty. Using the values in Table 1.2, the direct $\eta_b(1S)$ rate, integrated over the range $p_\perp > 8$ GeV, is [25]

$$\begin{aligned} \sigma(\eta_b; p_\perp > 8 \text{ GeV}) &\sim 40 \text{ nb} \qquad \text{MRSTLO} \\ &\sim 46 \text{ nb} \qquad \text{CTEQ5L}, \end{aligned} \tag{1.24}$$

while for h_b production

$$\begin{aligned} \sigma(h_b; p_\perp > 8 \text{ GeV}) &\sim 1.1 \text{ nb} \qquad \text{MRSTLO} \\ &\sim 1.1 \text{ nb} \qquad \text{CTEQ5L}. \end{aligned} \tag{1.25}$$

To give a simple estimate of the total rate, we can multiply by the ratio $\sigma(\Upsilon(1S))/\sigma(\Upsilon(1S); p_\perp > 8 \text{ GeV} \sim 6.5$, giving for the total cross sections

$$\begin{aligned} \sigma(\eta_b) &\sim 280 \text{ nb} \\ \sigma(h_b) &\sim 7 \text{ nb}. \end{aligned} \tag{1.26}$$

Due to the difficulty in observing h_b, it seems unlikely that it will be discovered at Run II.

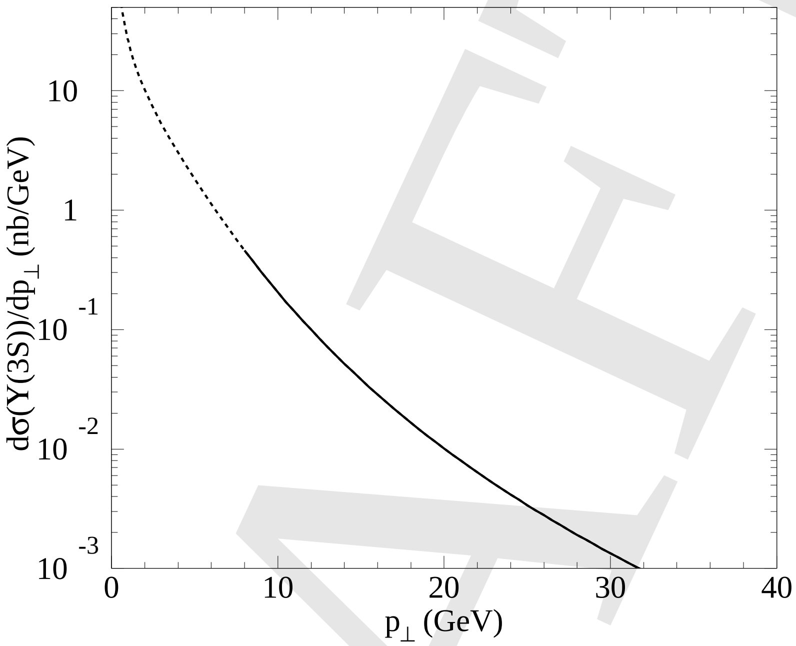

Figure 1.12: Differential cross section for $\Upsilon(3S)$ production at Run II. The rate is based on a rapidity range of $|y| \leq 0.4$.

1.2.2 Polarization in quarkonium production †

Measurements of the J/ψ and $\psi(2S)$ differential cross sections by CDF [28] separate the cross sections into those ψ mesons coming from b flavored hadron production and those originating from prompt production mechanisms. This separation is made by reconstructing the decay vertex of the J/ψ and $\psi(2S)$ mesons using the CDF Silicon Vertex (SVX). The fraction of J/ψ mesons coming from b flavored hadron production increases from 15% at 5 GeV/c to 40% at 18 GeV/c $P_T^{J/\psi}$. For $\psi(2S)$ mesons, a similar increase is seen in the range from 5 to 14 GeV/c. The prompt production of J/ψ mesons has three components: a feed-down from χ_c production, a feed-down from $\psi(2S)$ and a direct component. Only the latter occurs in the production of $\psi(2S)$ mesons. CDF has measured the fraction of prompt J/ψ mesons coming from χ_c production to be $(29.7 \pm 1.7 \pm 5.7)$% of the total prompt production [29]. ¿From the measured $\psi(2S)$ production cross section, the fraction of the prompt J/ψ's feeding down from $\psi(2S)$ meson decays is calculated to be 7 ± 2% at $P_T^{J/\psi} =$ 5 GeV/c and 15 ± 5% at $P_T^{J/\psi} = 18$ GeV/c. The fraction of directly produced J/ψ mesons is 64 ± 6%, independent of $P_T^{J/\psi}$ between 5 and 18 GeV/c.

† Authors: G. Feild, K.Sumorok, W. Trischuk

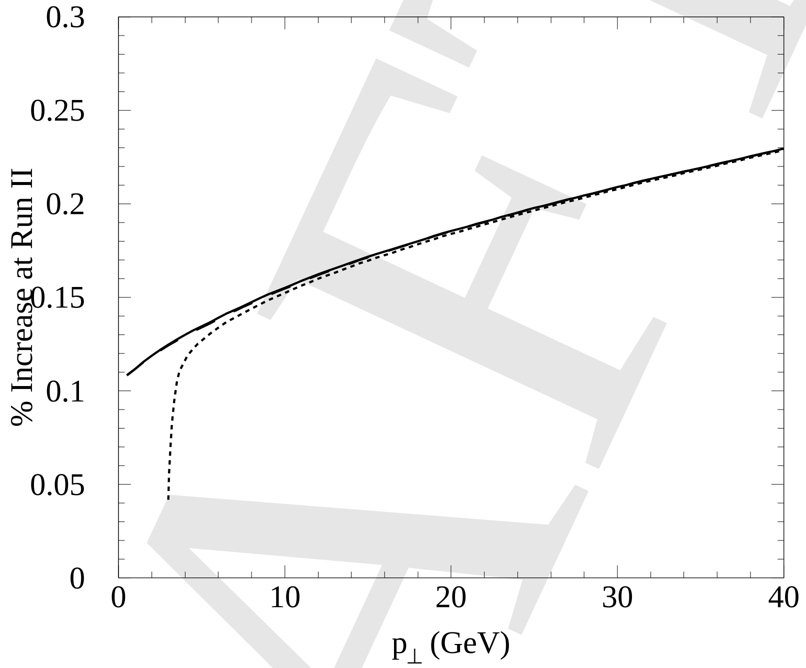

Figure 1.13: Percentage increase in Υ cross sections at Run II over Run I. The solid line is for $\Upsilon(1S)$, dotted for $\Upsilon(2S)$, and dashed for $\Upsilon(3S)$.

Having separated out the prompt J/ψ mesons coming from χ_c, both direct/prompt J/ψ and $\psi(2S)$ production appear to be ≈ 50 times higher than color singlet model (CSM) predictions [30].

1.2.2.1 NRQCD predictions for ψ meson polarization

Calculations based on the non-relativistic QCD (NRQCD) factorization formalism are able to explain this anomalous production [31], [32]. The model increases the prompt production cross section by including color-octet $c\bar{c}$ states ${}^1S_0^{(8)}$, ${}^3P_0^{(8)}$ and ${}^3S_1^{(8)}$ in the fragmentation process. The singlet term has a $1/P_T^8$ dependence, the terms ${}^1S_0^{(8)}$ and ${}^3P_0^{(8)}$ a $1/P_T^6$ dependence and the ${}^3S_1^{(8)}$ term a $1/P_T^4$. This last term, which fragments from a single gluon in production, dominates at high P_T. A single gluon is transversely polarized and NRQCD predicts this polarization is transfered to the J/ψ or $\psi(2S)$ mesons in the final state.

A consequence of this mechanism is that the direct prompt J/ψ mesons and the $\psi(2S)$ mesons will approach 100% transverse polarization at leading order in α_s for transverse momenta of $P_T^2 \gg m_c^2$ where m_c is the charm quark mass [32,34]. The observation of such a polarization would be an indication of the NRQCD fragmentation mechanism.

1.2.2.2 CDF polarisation measurements from Run I

CDF has made a measurement of the production polarization of J/ψ and $\psi(2S)$ (collectively ψ) mesons by analyzing decays into $\mu^+\mu^-$ [33]. Defining the angle θ by the direction of the μ^+ with respect to the ψ direction in the ψ center of mass frame, the normalized angular distribution $I(\theta)$ is given by

$$I(\theta) = \frac{3}{2(\alpha+3)}(1+\alpha\cos^2\theta). \tag{1.27}$$

Unpolarized ψ mesons would have $\alpha = 0$ whereas $\alpha = 1$ and -1 correspond to fully transverse and longitudinal polarizations respectively. The polarization parameter for prompt ψ production can be separated from the B-hadron decay component by fitting the proper decay length distribution for ψ candidates with both muons reconstructed in the SVX. Figure 1.14 shows the fitted polarization of J/ψ mesons obtained by CDF from prompt production and B-hadron decay compared with an NRQCD prediction for the prompt production [35]. The prediction for J/ψ meson polarization includes dilutions due to the contributions from χ_c and $\psi(2S)$ decays. Figure 1.15 shows the fitted polarization for $\psi(2S)$ mesons obtained by CDF from prompt production and B-hadron decay compared with NRQCD predictions for prompt production from [34] and [35].

1.2.2.3 Polarization precisions for Run II

The measurements in Run I were based on a luminosity of 110 pb^{-1}. Estimates for Run II are made assuming a factor of 20 increase in integrated luminosity, or 2 fb^{-1}. CDF is also planning to increase the yield of its dimuon trigger by 50% by lowering the P_T threshold. In addition, the SVX will have increased coverage along the beam line leading to better acceptance for dimuons fully reconstructed in the SVX. This is crucial for separation of prompt and B-hadron decay production in this measurement. Overall a factor of 50 increase in the effective statistics for a Run II is assumed in our projections. We have extrapolated to higher P_T using the fitted shape of the cross section below 20 GeV/c^2 in order to predict the number of events in a given P_T bin and estimated errors scaling statistics from Run I measurements. In Run I systematic uncertainties on the polarization measurement were small compared to the statistical errors. We anticipate that the systematics can be improved with the Run II data samples, but even if this is not the case systematics should still be negligible at the highest P_Ts. Figure 1.16 shows the expected precision for a polarization measurement in Run II of promptly produced J/ψ and $\psi(2S)$ mesons. Relative to Run I the P_T range should be extended and the error bars on the measurement reduced. The points are slightly scattered about zero to ease visibility.

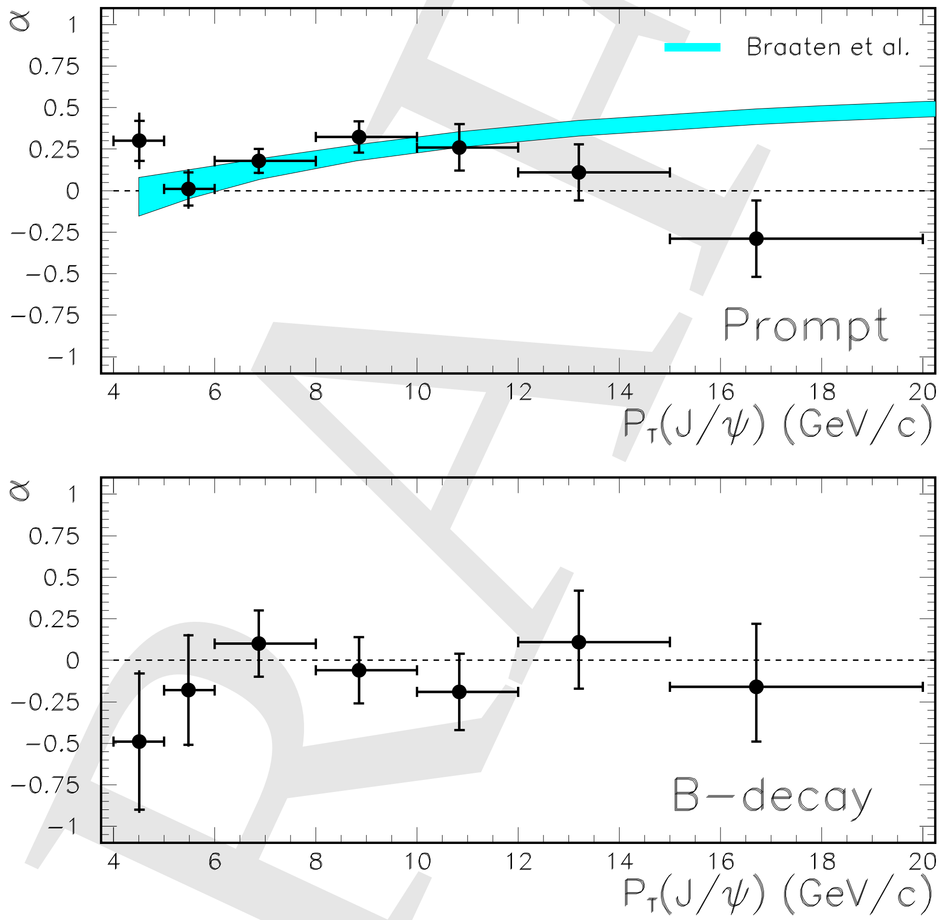

Figure 1.14: The fitted polarization of J/ψ mesons from prompt production and B-hadron decay. The shaded curve shows an NRQCD prediction from [35].

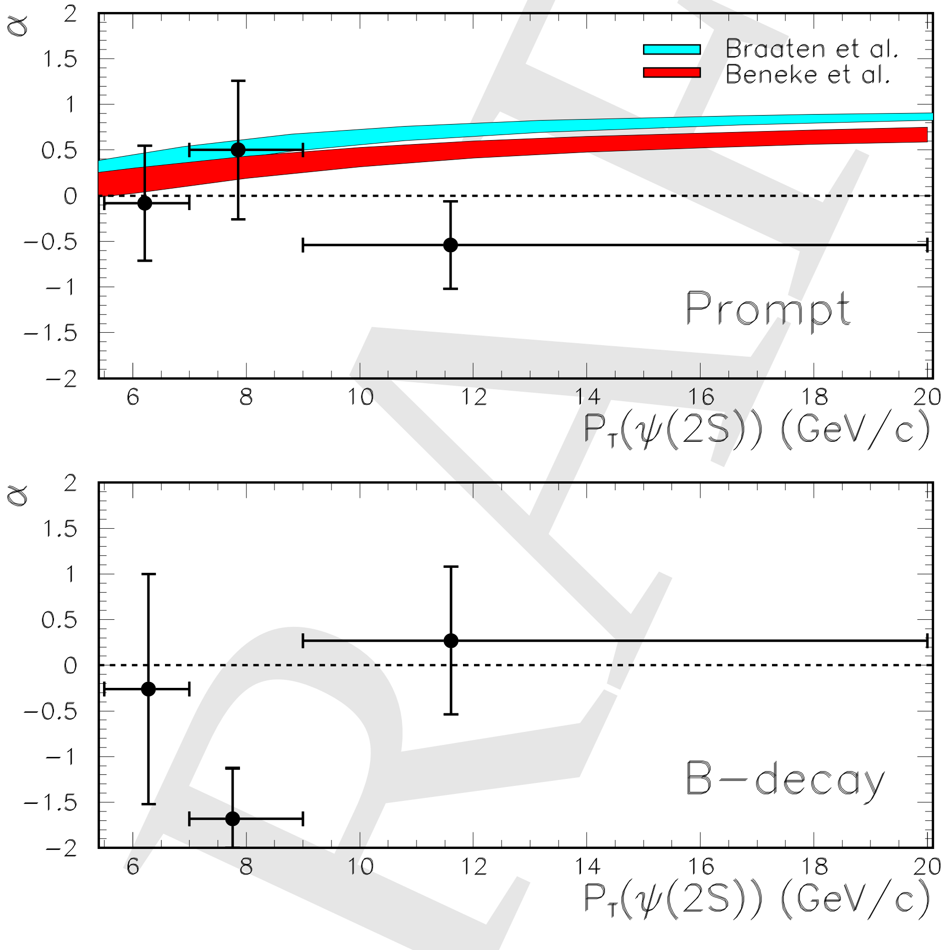

Figure 1.15: The fitted polarization of $\psi(2S)$ mesons from prompt production and B-hadron decay. The shaded curves are NRQCD predictions from [34], [35].

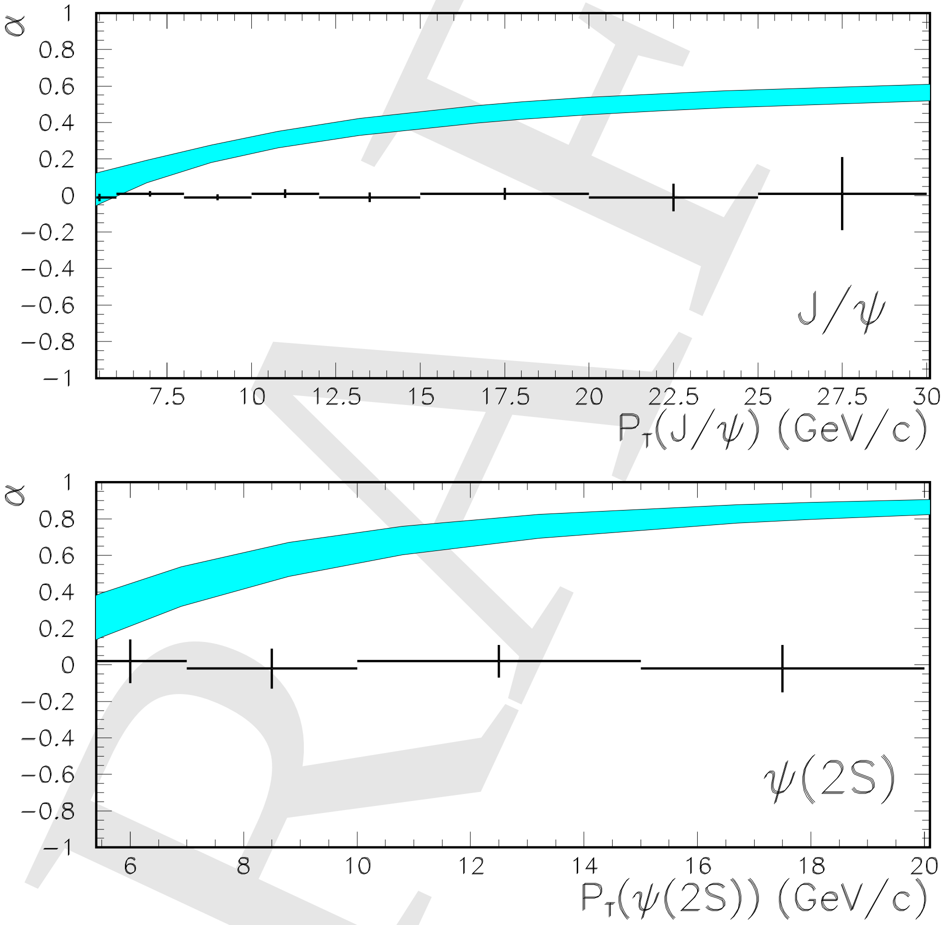

Figure 1.16: The expected precision for a polarization measurement in Run II of promptly produced J/ψ and $\psi(2S)$ mesons. The shaded curves are NRQCD predictions from [35].

1.3 Production and decay of states containing two heavy quarks

1.3.1 Spectroscopy of $b\bar{c}$ and QQq

This section should give a list of references and needs to be written

1.3.2 Production of states containing two heavy quarks †

The production of a B_c proceeds in three steps. First, a $\bar{b}$ and c with small relative momentum are created by a parton collision. Second, the $\bar{b}$ and c bind to form the B_c or one of its excited states below the BD threshold. Third, the excited states all cascade down to the ground state B_c via hadronic or electromagnetic transition. Thus, the total production cross section for B_c is the sum of the direct production cross sections for B_c and its excited states.

The production of S-wave $\bar{b}c$ states is simpler than for quarkonium, because we need only consider the production of $\bar{b}c$ in a color-singlet S-wave state. There is no kinematical suppression of color-singlet contributions at large p_T analogous to the suppression of $gg \to c\bar{c}_1(^3S_1) + g$ by m_Q^4/p_T^4 . There is also no kinematical enhancement of the color-octet contribution analogous to the enhancement of $c\bar{c}_8(^3S_1)$ at large p_T due to the order α_s fragmentation process $g \to c\bar{c}_8(^3S_1)$. The color-octet contributions are uniformly suppressed by v^4, where v is the typical relative velocity of the $\bar{b}$ and c. Thus the direct cross section of B_c and other S-wave can be predicted with an absolute normalization that is determined by the wavefunction at the origin for the bound state.

The production of the P-wave states is just as complicated as for quarkonium, because there is a color-octet S-wave contribution that is the same order in v as the color-singlet contribution. The color-singlet NRQCD matrix for a given P-wave state can be expressed in terms of the wavefunction from potential models. The color-octet NRQCD matrix element can perhaps be estimated by interpolating between the corresponding matrix elements in charmonium and bottomonium. The color-octet contributions to the cross sections for P-wave B_c states have not yet been calculated.

The leading-order mechanisms for creating the $\bar{b}c$ pair that bind to form a B_c meson are the order-α_s^4 parton processes $q\bar{q}, gg \to (\bar{b}c) + b\bar{c}$. At the Tevatron, the gg contribution dominates. The $q\bar{q}$ contribution is smaller by a factor that ranges from ????? for $p_T \sim M_{B_c}$ to ????? at $p_T = 30$ GeV. In Figure 1, we show the cross sections for direct production of $B_c^\pm$ and total production of $B_c^\pm$ at central rapidity $|y| < 1$ at the Tevatron with $\sqrt{s} = 2.0$ TeV. The cross-sections are summed over B_c^+ and B_c^-. The total cross section includes the contributions from the 1S, 2S, and 3S states and the color-singlet contributions to the cross sections for the 1P, 2P, and 3P states. The color-singlet contributions to the P-wave states account for about ????? % of the total cross sections, and the uncalculated color-octet contributions could be comparable in magnitude. At $\sqrt{s} = 1.8$ TeV, the differential cross

† Author: Eric Braaten

section $d\sigma/dy$ at central rapidity has been calculated to be ????? nb for $p_T > 5$ GeV and ????? nb integrated over all p_T [Reference?]. At $\sqrt{s} = 2.0$ TeV, the cross section is larger by about a factor of ?????.

The dominant error in the calculation probably comes from higher order QCD corrections. A lower bound on the error can be obtained by varying the factorization and renormalization scales by a factor of 2 from some central value. Taking the central value to be $\sqrt{m_b^2 + p_T^2}$, the error estimate ranges from a factor of ????? at low p_T to a factor of ????? at the highest p_T's shown. This is probably an underestimate because there are significant contributions involving particles that are only off-shell by amounts of order m_c.

At large p_T, the leading-order cross section for B_c production can be expressed in a much simpler form. It can be factored into the leading-order cross section for producing $\bar{b}$ and the fragmentation function for the $\bar{b}$ to form a B_c:

$$d\sigma[B_c(P)] \approx d\sigma[\bar{b}(P/z)] \otimes D_{\bar{b}\to B_c}(z)$$

Numerical studies have shown that this fragmentation approximation becomes accurate to better than 10% for $p_T >$????? GeV. Thus at larger values of p_T, the ratio of the cross sections for B_c and b is probing the fragmentation function for $\bar{b} \to B_c$. In Figure 2, we plot the ratio of the leading-order differential cross sections for B_c (summed over $\bar{b}c$ mesons) and for $\bar{b}$ as a function of p_T. We compare it to the corresponding ratio with the numerator computed using the fragmentation approximation. We see that ...

SUGGESTED FIGURES:

Figure 1. The differential cross section $d\sigma/dp_t dy$ for direct production (lower curve) and total production (upper curve) of $B_c^\pm$ at central rapidity at the Tevatron at $\sqrt{s} = 2.0$ GeV.

Figure 2. Ratio of the differential cross sections for $p\bar{p} \to B_c + X$ (summed over all $b\bar{c}$ mesons) and $p\bar{p} \to b + X$ at central rapidity as a function of p_T. At large p_T, it approaches the fragmentation probability for $\bar{b} \to B_c$.

1.3.3 Production of B_c and QQq[†]

The observation of approximate 20 events of B_c-meson in the $B_c \to J/\psi l\nu$ decay mode at Tevatron (CDF-collaboration) [51] demonstrates the possibility of experimental study of doubly heavy systems with open flavors. The small value of the production cross-sections for such particles is due the presence of two pair of heavy quarks in the final state. This gives, for example, for B_c-meson

$$\sigma(B_c)/\sigma(B) \sim 10^{-3}.$$

It is worth mentioning that the production mechanism of a double heavy particle with open flavor differs in an essential way from that of a heavy particle with hidden flavor.

[†]Author: A. Likhoded

The production mechanism of the particle under consideration was studied in details in the series of papers [52] in the framework of pQCD O(α_s^4) calculations. The long-distance effects were taken into account by means of nonrelativistic wave function of B_c-meson or diquark in Double Heavy Baryon (DHB) (ccq, bcq, bbq). As a result the yield for such particles is proportional to simple factor

$$\alpha_s^4 |R_s(0)|^2,$$

where $\alpha_s(\mu)$ is the strong coupling constant and $R_s(0)$ is the wave function at the origin. The main uncertainties in the theoretical prediction arise due to this factor. For example, the variation of the scale μ from m_c up to $2(m_c + m_b)$ in the calculations of the B_c cross-section gives a factor of 7 in the cross-section. An additional ambiguity is due to the uncertainties in the value of the wave function and the c-quark mass. This leads to the uncertainty smaller than a factor of 2.

The results of exact O(α_s^4) calculation for $d\sigma/dp_T$ of B_c-meson, Ξ_{cc}, Ξ_{bc} and Ξ_{bb}-baryons are presented in Fig. 1.17.

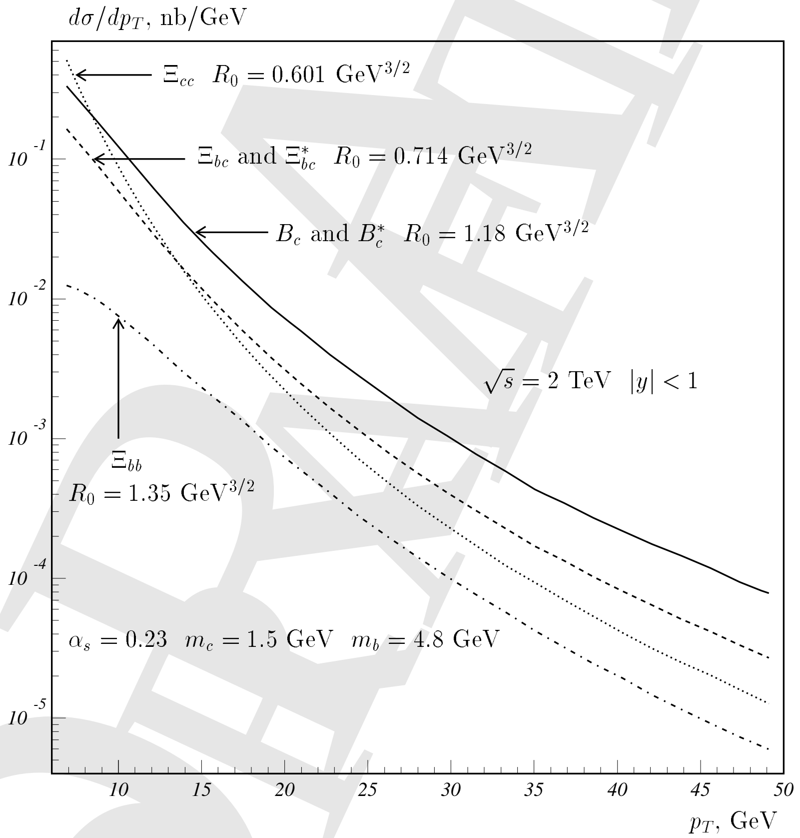

Figure 1.17: Differential cross section for QQq and B_c production

In our calculations we used the following values of parameters

$$m_c = 1.5 \text{ GeV}, \; m_b = 4.8 \text{ GeV}, \; \alpha_s = 0.23$$

$$R_{1S}^{B_c}(0) = 1.18 \text{ GeV}^{3/2}, \; R_{1S}^{cc}(0) = 0.601 \text{ GeV}^{3/2}, \; R_{1S}^{bc}(0) = 0.714 \text{ GeV}^{3/2}, \; R_{1S}^{bb}(0) = 1.35 \text{ GeV}^{3/2}.$$

for $p_T > 6$ GeV and $|y| < 1$ at the Tevatron energies (1.8 TeV). For the B_c-meson cross-section we take into account the production of $1S$-states (B_c^* and B_c) only. The sum over $1S$- and $2S$-wave and the P-wave ($\sim 10\%$) states gives the following value of B_c-production cross-section for $p_T > 6$GeV and $|y| < 1$:

$$\sigma_{th}(B_c^+) = 2.5 \text{ nb.}$$

This value should be compared with experimental value [?]

$$\sigma_{exp.} \sim 10 \pm 6 \text{ nb}$$

obtained for $Br(B_c^+ \to J/\Psi + l\nu) = 2.5 \pm 0.5 \times 10^{-2}$ The cross-section integrated over p_T up to $p_{T_{min}}$ for B_c and DHB is shown in Fig. 1.18

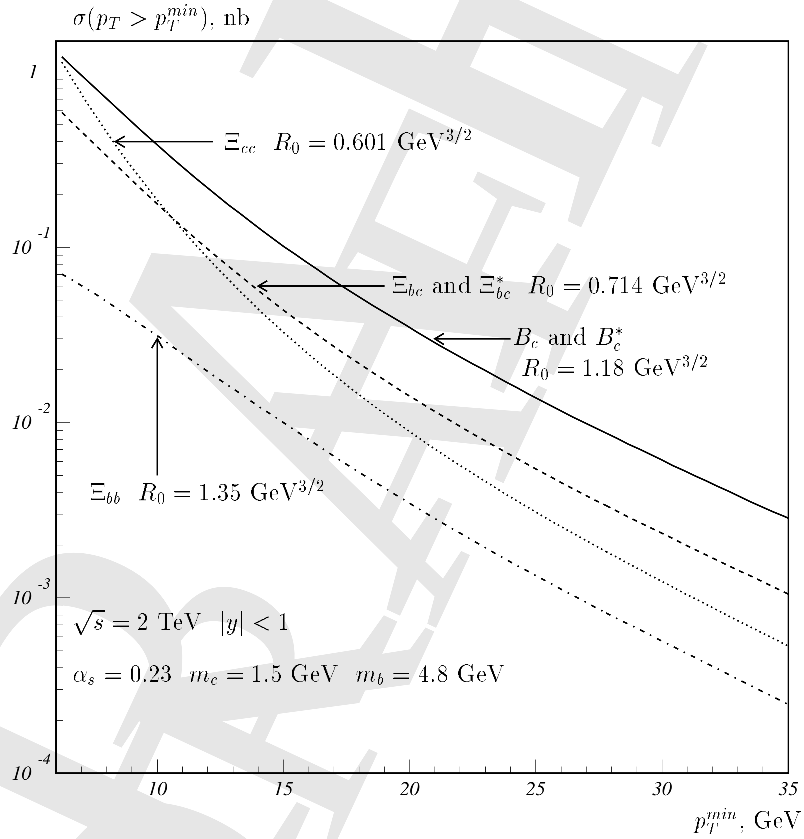

Figure 1.18: Integrated cross section for QQq and B_c production

It should be mentioned that in our calculation we use value $\alpha_s = 0.23$ which allows to describe the experimental data of the OPAL Collaboration on the additional production of the $c\bar{c}$-pair in the e^+e^--annihilation [52].

1.3.3.1 Ξ_{bc} at Tevatron

As it was mentioned above, the Ξ_{bc} cross-section is calculated by taking into account the same set of diagrams as in the case of the B_c-production. The difference is that the bc-diquark is produced in color antitriplet state and the diquark wave function at the origin has another numerical value. So, the ratio $\sigma(B_c)/\sigma(\Xi_{bc})$ does not depend on α_s^4, which gives us the bulk of the uncertainty in the predictions for the Ξ_{bc} cross-section. Using the bc-diquark wave function value [54] of

$$R_S^{bc}(0) = 0.714\ \mathrm{GeV}^{3/2}$$

one can get the following estimates

$$\sigma(B_c)/\sigma(\Xi_{bc}) = 2.$$

So, taking into account cascade decays of exited states we can make the following prediction for Ξ_{bc} production cross-section for $p_T > 6$GeV and $|y| < 1$

$$\sigma(\Xi_{bc}) = 1.5\ nb,$$

or, keeping in mind the experimental value of cross section for B_c, we get

$$\sigma(\Xi_{bc}) = 5 \pm 3\ nb.$$

This value corresponds to more than 10^5 events with Ξ_{bc}-baryons for integrated luminosity of $100 \div 150\ \ pb^{-1}$ in the considered kinematical region. After the upgrade of Tevatron one expects the increase of this number by factor of 20.

It should be noted that there are no as good unambiguous predictions for all others DHB (cc or bb) as for bc-case. In any case, it follows from our predictions that one can expect almost the same number of Ξ_{cc} as that of Ξ_{bc} in the kinematical region of $p_T >$6 GeV and $|y| < 1$. The total number of Ξ_{bb} events will be about a factor of ten less.

1.3.4 Theoretical Status of B_c Decays and Lifetime†

Decays of the long-lived heavy meson B_c, containing two heavy quarks of different flavors, were considered in the pioneering paper written by Bjorken in 1986 [57]. The report was devoted to a unified view of the decays of hadrons with heavy quarks: the mesons and baryons with a single heavy quark, the B_c meson, the baryons with two and three heavy quarks. A major effort was recently directed to study the long-lived doubly heavy hadrons on the basis of modern understanding of QCD dynamics in the weak decays of heavy flavors. The modern theoretical tools are the Operator Product Expansion, sum rules of QCD and NRQCD, and potential models adjusted using data from hadrons with a single heavy quark. Surprisingly, Bjorken's estimates of total widths and various branching fractions are close to what is evaluated in a more strict manner. At present we are tending to study some subtle effects caused by the influence of strong forces onto the weak decays of heavy quarks, which determines our understanding a probable fine extraction of CP-violation in the heavy quark sector.

Various hadronic matrix elements enter in the description of weak decays. So, measuring the lifetimes and branching ratios implies the investigation of quark confinement by the

†Authors: V.V.Kiselev, A.K.Likhoded

strong interactions, which is important in the evaluation of pure quark characteristics: masses and mixing angles in the CKM matrix, all of which enter as constraints on the physics beyond the Standard Model. More collection of hadrons with heavy quarks provides more accuracy and confidence in the understanding of QCD dynamics and isolation of bare quark values.

A new laboratory for such investigations is a doubly heavy long-lived quarkonium B_c recently observed for the first time by the CDF Collaboration [58]. The measured B_c lifetime is equal to

$$\tau[B_c] = 0.46^{+0.18}_{-0.16} \pm 0.03 \text{ ps} .$$

The B_c meson allows us to use such advantages like the nonrelativistic motion of $\bar{b}$ and c quarks similar to what is know in the heavy quarkonia $\bar{b}b$ and $\bar{c}c$, and suppression of light degrees of freedom: the quark-gluon sea is small in the heavy quarkonia. These two physical conditions imply two small expansion parameters for B_c:

- the relative velocity of quarks v,
- the ratio of confinement scale to the heavy quark mass Λ_{QCD}/m_Q.

The double expansion in v and $1/m_Q$ generalizes the HQET approach [59] to what is called as NRQCD [60]. Moreover, the energy release in the heavy quark decays determines the $1/m_Q$ parameter to be the appropriate quantity for the Operator Product Expansion (OPE) and justifies the use of potential models (PM) in the calculations of hadronic matrix elements, too. The same arguments ensure the applicability of sum rules (SR) of QCD and NRQCD.

The B_c decays were, at first, calculated in the PM [61], wherein the variation of techniques results in close estimates after the adjustment on the semileptonic decays of B mesons. The OPE evaluation of inclusive decays gave the lifetime and widths [62], which agree with PM, if one sums up the dominating exclusive modes. That was quite unexpected, when the SR of QCD resulted in the semileptonic B_c widths [63], which are one order of magnitude less than those of PM and OPE. The reason was the valuable role of Coulomb corrections, that implies the summation of α_s/v corrections significant in the heavy quarkonia, i.e. in the B_c [64,65]. At present, all of mentioned approaches give the close results for the lifetime and decay modes of B_c at similar sets of parameters. Nevertheless, various dynamical questions remain open:

- What is the appropriate normalization point of nonleptonic weak lagrangian in the B_c decays, which basically determines its lifetime?
- What are the values of masses for the charmed and beauty quarks?
- What are the implications of NRQCD symmetries for the form factors of B_c decays and partial widths?
- How consistent is our understanding of hadronic matrix elements, characterizing the B_c decays, with the data on the other heavy hadrons?

In the present short review of B_c decays we summarize the theoretical predictions and discuss how direct experimental measurements can answer the questions above.

1.3.4.1 B_c lifetime and inclusive decay rates

The B_c-meson decay processes can be subdivided into three classes:

1) the $\bar{b}$-quark decay with a spectator c-quark,

2) the c-quark decay with a spectator $\bar{b}$-quark and

3) the annihilation channel $B_c^+ \to l^+\nu_l(c\bar{s}, u\bar{s})$, where $l = e,\ \mu,\ \tau$.

In the $\bar{b} \to \bar{c}c\bar{s}$ decays one separates also the Pauli interference with the c-quark from the initial state. In accordance with the given classification, the total width is the sum over the partial widths

$$\Gamma(B_c \to X) = \Gamma(b \to X) + \Gamma(c \to X) + \Gamma(\text{ann.}) + \Gamma(\text{PI})\ . \tag{1.28}$$

For the annihilation channel the $\Gamma(\text{ann.})$ width can be reliably estimated in the framework of inclusive approach, where one takes the sum of the leptonic and quark decay modes with account for the hard gluon corrections to the effective four-quark interaction of weak currents. These corrections result in the factor of $a_1 = 1.22 \pm 0.04$. The width is expressed through the leptonic constant of $f_{B_c} \approx 400$ MeV. This estimate of the quark-contribution does not depend on a hadronization model, since a large energy release of the order of the meson mass takes place. From the following expression, one can see that the contribution by light leptons and quarks can be neglected,

$$\Gamma(\text{ann.}) = \sum_{i=\tau,c} \frac{G_F^2}{8\pi}|V_{bc}|^2 f_{B_c}^2 M m_i^2 (1 - m_i^2/m_{Bc}^2)^2 \cdot C_i\ , \tag{1.29}$$

where $C_\tau = 1$ for the $\tau^+\nu_\tau$-channel and $C_c = 3|V_{cs}|^2 a_1^2$ for the $c\bar{s}$-channel.

As for the non-annihilation decays, in the approach of the Operator Product Expansion for the quark currents of weak decays [62], one takes into account the α_s-corrections to the free quark decays and uses the quark-hadron duality for the final states. Then one considers the matrix element for the transition operator over the bound meson state. The latter allows one also to take into account the effects caused by the motion and virtuality of decaying quark inside the meson because of the interaction with the spectator. In this way the $\bar{b} \to \bar{c}c\bar{s}$ decay mode turns out to be suppressed almost completely due to the Pauli interference with the charm quark from the initial state. Besides, the c-quark decays with the spectator $\bar{b}$-quark are essentially suppressed in comparison with the free quark decays because of a large bound energy in the initial state.

In the framework of exclusive approach, it is necessary to sum up widths of different decay modes calculated in the potential models [61]. While considering the semileptonic decays due to the $\bar{b} \to \bar{c}l^+\nu_l$ and $c \to sl^+\nu_l$ transitions, one finds that in the former decays the hadronic final state is practically saturated by the lightest bound $1S$-state in the $(\bar{c}c)$-system, i.e. by the η_c and J/ψ particles, and in the latter decays, the $1S$-states in the $(\bar{b}s)$-system, i.e. B_s and B_s^*, can only enter the accessible energetic gap.

Table 1.3: The branching ratios of the B_c decay modes calculated in the framework of inclusive OPE approach and summing up the exclusive modes in the potential model [61,65] and in the sum rules of QCD and NRQCD [65].

B_c decay mode	OPE, %	PM, %	SR, %
$\bar{b} \to \bar{c} l^+ \nu_l$	3.9 ± 1.0	3.7 ± 0.9	2.9 ± 0.3
$\bar{b} \to \bar{c} u \bar{d}$	16.2 ± 4.1	16.7 ± 4.2	13.1 ± 1.3
$\sum \bar{b} \to \bar{c}$	25.0 ± 6.2	25.0 ± 6.2	19.6 ± 1.9
$c \to s l^+ \nu_l$	8.5 ± 2.1	10.1 ± 2.5	9.0 ± 0.9
$c \to s u \bar{d}$	47.3 ± 11.8	45.4 ± 11.4	54.0 ± 5.4
$\sum c \to s$	64.3 ± 16.1	65.6 ± 16.4	72.0 ± 7.2
$B_c^+ \to \tau^+ \nu_\tau$	2.9 ± 0.7	2.0 ± 0.5	1.8 ± 0.2
$B_c^+ \to c\bar{s}$	7.2 ± 1.8	7.2 ± 1.8	6.6 ± 0.7

Further, the $\bar{b} \to \bar{c} u \bar{d}$ channel, for example, can be calculated through the given decay width of $\bar{b} \to \bar{c} l^+ \nu_l$ with account for the color factor and hard gluon corrections to the four-quark interaction. It can be also obtained as a sum over the widths of decays with the $(u\bar{d})$-system bound states.

The results of calculation for the total B_c width in the inclusive OPE and exclusive PM approaches give the values consistent with each other, if one takes into account the most significant uncertainty related to the choice of quark masses (especially for the charm quark), so that finally, we have

$$\tau(B_c^+) = 0.55 \pm 0.15 \text{ ps}, \tag{1.30}$$

which agrees with the measured value of B_c lifetime.

The OPE estimates of inclusive decay rates agree with recent calculations in the sum rules of QCD and NRQCD [65], where one assumed the saturation of hadronic final states by the ground levels in the $c\bar{c}$ and $b\bar{s}$ systems as well as the factorization allowing one to relate the semileptonic and hadronic decay modes. The coulomb-like corrections in the heavy quarkonia states play an essential role in the B_c decays and allow one to remove the disagreement between the estimates in sum rules and OPE. In contrast to OPE, where the basic uncertainty is given by the variation of heavy quark masses, these parameters are fixed by the two-point sum rules for bottomonia and charmonia, so that the accuracy of SR calculations for the total width of B_c is determined by the choice of scale μ for the hadronic weak lagrangian in decays of charmed quark. We show this dependence in Figure 1.19, where $\frac{m_c}{2} < \mu < m_c$ and the dark shaded region corresponds to the scales preferred by data on the charmed meson lifetimes.

Thus, we suppose the preferable choice of scale in the $c \to s$ decays of B_c to be equal to $\mu_{B_c}^2 \approx (0.85 \text{ GeV})^2$, and at $a_1(\mu_{B_c}) = 1.20$ in the charmed quark decays we predict [65]

$$\tau[B_c] = 0.48 \pm 0.05 \text{ ps}. \tag{1.31}$$

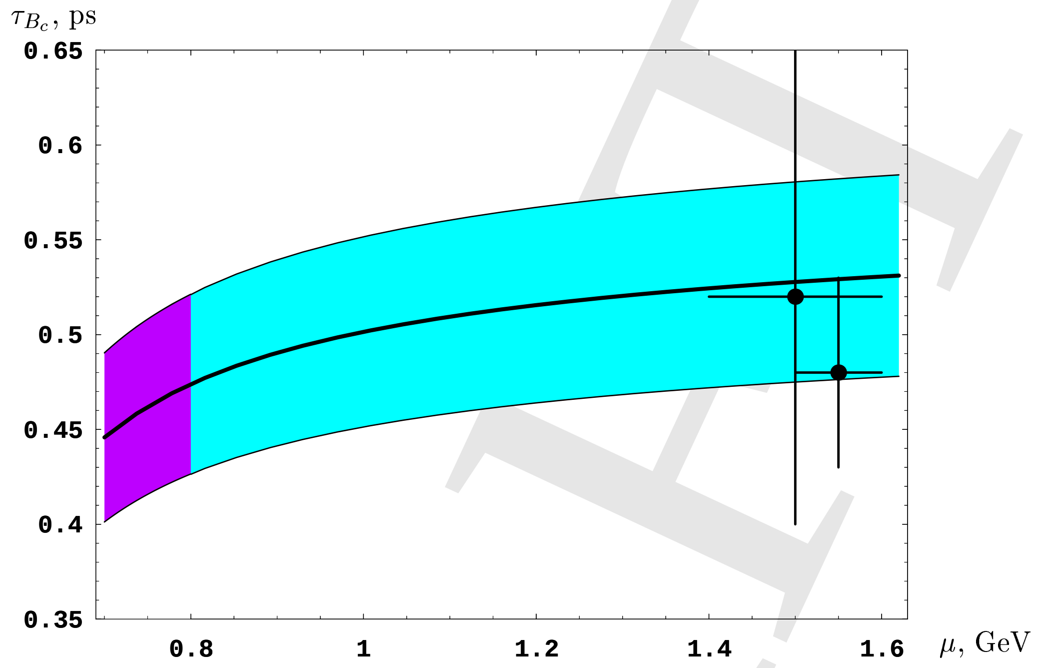

Figure 1.19: The B_c lifetime calculated in QCD sum rules versus the scale of hadronic weak lagrangian. The shaded region shows the uncertainty of estimates, the dark shaded region is the preferable choice as given by the lifetimes of charmed mesons. The dots represent the values in OPE approach taken from refs. [62].

1.3.4.2 Semileptonic and leptonic modes

The semileptonic decay rates are underestimated in the QCD SR approach of ref. [63], because large coulomb-like corrections were not taken into account. The recent analysis of SR in [64,65] decreased the uncertainty, so that the estimates agree with the calculations in the potential models (see Table 1.4).

In practice, the most constructive information is given by the ψ mode, since this charmonium is clearly detected in experiments due to the pure leptonic decays [58].

1.3.4.3 Relations between the form factors

In the limit of infinitely heavy quark mass, the NRQCD and HQET lagrangians possess the spin symmetry, since the heavy quark spin is decoupled in the leading approximation. The most familiar implication of such the symmetry is the common Isgur-Wise function determining the form factors in the semileptonic decays of singly heavy hadrons. In contrast to the weak decays with the light spectator quark, the B_c decays to both the charmonia ψ and η_c and $B_s^{(*)}$ involve the heavy spectator, so that the spin symmetry works only at the recoil momenta close to zero, where the spectator enters the heavy hadron in the final state with no hard gluon rescattering. Hence, in a strict consideration we expect the relations between the form factors in the vicinity of zero recoil. The normalization of common form

Table 1.4: The widths of semileptonic B_c decay modes and the branching fractions calculated in QCD SR at $\tau_{B_c} = 0.46$ ps. The accuracy is about 10%.

mode	Γ, 10^{-14} GeV	BR, %
$B_s e^+ \nu_e$	5.8	4.0
$B_s^* e^+ \nu_e$	7.2	5.0
$\eta_c e^+ \nu_e$	1.1	0.75
$\eta_c \tau^+ \nu_\tau$	0.33	0.22
$\psi e^+ \nu_e$	2.8	2.1
$\psi \tau^+ \nu_\tau$	0.7	0.51

factor is not fixed, as was in decays of hadrons with a single heavy quark, since the heavy quarkonia wave-functions are flavor-dependent. Nevertheless, in practice, the ratios of form factors as fixed at a given zero recoil point are broken only by the different dependence on the transfer squared, that is not significant in real numerical estimates in the restricted region of physical phase space.

As for the implications of spin symmetry for the form factors of decay, in the soft limit for the transitions $B_c^+ \to \psi(\eta_c)e^+\nu$

$$\begin{aligned} v_1^\mu &\neq v_2^\mu, \\ w &= v_1 \cdot v_2 \to 1, \end{aligned} \tag{1.32}$$

where $v_{1,2}^\mu = p_{1,2}^\mu / \sqrt{p_{1,2}^2}$ are the four-velocities of heavy quarkonia in the initial and final states, we derive the relations [65]

$$\begin{aligned} f_+(c_1^P \cdot \mathcal{M}_2 - c_2^P \mathcal{M}_1) - f_-(c_1^P \cdot \mathcal{M}_2 + c_2^P \cdot \mathcal{M}_1) &= 0, \\ F_0^A \cdot c_V - 2c_\epsilon \cdot F_V \mathcal{M}_1 \mathcal{M}_2 &= 0, \\ F_0^A(c_1 + c_2) - c_\epsilon \mathcal{M}_1 (F_+^A(\mathcal{M}_1 + \mathcal{M}_2) + F_-^A(\mathcal{M}_1 - \mathcal{M}_2)) &= 0, \\ F_0^A c_1^P + c_\epsilon \cdot \mathcal{M}_1 (f_+ + f_-) &= 0, \end{aligned} \tag{1.33}$$

where

$$\begin{aligned} c_\epsilon &= -2, \\ c_1 &= -\frac{m_3(3m_1 + m_3)}{4m_1 m_2}, \\ c_2 &= \frac{1}{4m_1 m_2}(4m_1 m_2 + m_1 m_3 + 2m_2 m_3 + m_3^2), \\ c_V &= -\frac{1}{2m_1 m_2}(2m_1 m_2 + m_1 m_3 + m_2 m_3), \\ c_1^P &= 1 + \frac{m_3}{2m_1} - \frac{m_3}{2m_2}, \\ c_2^P &= 1 - \frac{m_3}{2m_1} + \frac{m_3}{2m_2}, \end{aligned} \tag{1.34}$$

so that $m_1 = m_b$ is the mass of decaying quark, $m_2 = m_3 = m_c$, $\mathcal{M}_1 = m_1 + m_2$, $\mathcal{M}_2 = m_2 + m_3$, and the form factors are defined by the equations

$$\langle \eta_c(p_2)|V_\mu|B_c(p_1)\rangle = f_+(p_1+p_2)_\mu + f_- q_\mu, \tag{1.35}$$

$$\frac{1}{i}\langle J/\psi(p_2)|V_\mu|B_c(p_1)\rangle = iF_V \epsilon_{\mu\nu\alpha\beta}\epsilon^{*\nu}(p_1+p_2)^\alpha q^\beta, \tag{1.36}$$

$$\frac{1}{i}\langle J/\psi(p_2)|A_\mu|B_c(p_1)\rangle = F_0^A\epsilon^*_\mu + F_+^A(\epsilon^*\cdot p_1)(p_1+p_2)_\mu + F_-^A(\epsilon^*\cdot p_1)q_\mu, \tag{1.37}$$

where $q_\mu = (p_1 - p_2)_\mu$ and $\epsilon^\mu = \epsilon^\mu(p_2)$ is the polarization vector of J/ψ-meson. V_μ and A_μ are the flavor changing vector and axial electroweak currents. The SR estimates of form factors show a good agreement with the relations, whereas the deviations can be basically caused by the difference in the q^2-evolution of form factors from the zero recoil point, that can be neglected within the accuracy of SR method.

In the same limit for the modes of $B_c^+ \to B_s^{(*)}e^+\nu$ we find that the ambiguity in the 'light quark propagator'[3] restricts the number of relations, and we derive

$$\begin{aligned} f_+(c_1^P\cdot\mathcal{M}_2 - c_2^P\mathcal{M}_1) - f_-(c_1^P\cdot\mathcal{M}_2 + c_2^P\cdot\mathcal{M}_1) &= 0,\\ F_0^A\cdot c_V - 2c_\epsilon\cdot F_V\mathcal{M}_1\mathcal{M}_2 &= 0,\\ F_0^A c_1^P + c_\epsilon\cdot\mathcal{M}_1(f_+ + f_-) &= 0, \end{aligned} \tag{1.38}$$

where

$$\begin{aligned} c_\epsilon &= -2,\\ c_V &= -1 - \tilde{B} - \frac{m_3}{2m_1},\\ c_1^P &= 1 - \tilde{B} + \frac{m_3}{2m_1},\\ c_2^P &= 1 + \tilde{B} - \frac{m_3}{2m_1}. \end{aligned} \tag{1.39}$$

so that $m_1 = m_c$ is the mass of decaying quark, $m_2 = m_s$, $m_3 = m_b$, $\mathcal{M}_1 = m_1 + m_2$, $\mathcal{M}_2 = m_2 + m_3$. The parameter $\tilde{B}$ has the form

$$\tilde{B} = -\frac{2m_1 + m_3}{2m_1} + \frac{4m_3(m_1+m_3)F_V}{F_0^A}. \tag{1.40}$$

The $1/m_Q$-deviations from the symmetry relations in the decays of $B_c^+ \to B_s^{(*)}e^+\nu$ are about 10-15 %, as found in the QCD sum rules.

Note, that the combinations of relations given above reproduce the results of [66], wherein the only equality was found for each mode above at $v_1 = v_2$.

[3] Strictly, we deal with the uncertainty in the spin structure of amplitude because of light degrees of freedom.

1.3.4.4 Leptonic decays

The dominant leptonic decay of B_c is given by the $\tau\nu_\tau$ mode (see Table 1.3). However, it has a low experimental efficiency of detection because of hadronic background in the τ decays or a missing energy. Recently, in refs. [67] the enhancement of muon and electron channels in the radiative modes was studied. The additional photon allows one to remove the helicity suppression for the leptonic decay of pseudoscalar particle, which leads, say, to the double increase of muonic mode.

1.3.4.5 Nonleptonic modes

In comparison with the the inclusive non-leptonic widths, which can be estimated in the framework of quark-hadron duality (see Table 1.3), the calculations of exclusive modes usually involves the approximation of factorization [69], which, as expected, can be quite accurate for the B_c, since the quark-gluon sea is suppressed in the heavy quarkonium. Thus, the important parameters are the factors a_1 and a_2 in the non-leptonic weak lagrangian, which depend on the normalization point suitable for the B_c decays.

The QCD SR estimates for the nonleptonic decays of charmed quark in B_c give the widths represented in Table 1.5 [65] and agree with the values predicted by the potential models.

Table 1.5: The widths of nonleptonic B_c decay modes and branching fractions calculated at $\tau_{B_c} = 0.46$ ps. We put a_1=1.26.

mode	Γ, 10^{-14} GeV	BR, %
$B_s\pi^+$	15.8 a_1^2	17.5
$B_s\rho^+$	6.7 a_1^2	7.4
$B_s^*\pi^+$	6.2 a_1^2	6.9
$B_s^*\rho^+$	20.0 a_1^2	22.2

At large recoils as in $B_c^+ \to \psi\pi^+(\rho^+)$, the spectator picture of transition can be broken by the hard gluon exchanges, that enlarge the estimates of potential models by a factor of 4 [68]. The corresponding estimates in the factorization approach are determined by the leptonic constants and the QCD coupling constant at the virtualities of hard gluon (see Figure 1.20), so that

$$\Gamma(B_c^+ \to \psi\pi^+) = G_F^2|V_{bc}|^2\, \frac{128\pi\alpha_s^2}{81}\left(\frac{M+m}{M-m}\right)^3 \frac{f_\pi^2 \tilde{f}_{B_c}^2 \tilde{f}_\psi^2 M^3}{(M-m)^2 m^2}\, a_1^2, \tag{1.41}$$

$$\frac{\Gamma(B_c^+ \to \eta_c\pi^+)}{\Gamma(B_c^+ \to \psi\pi^+)} = \frac{[3M^2 - 2Mm + m^2]^2}{4M^4}, \tag{1.42}$$

where $m = m_\psi$ or $m = m_{\eta_c}$, respectively. Numerically, one finds the values represented in Table 1.6, so that the matrix element is <u>twice enhanced</u> in comparison with that of the potential model value due to the contribution of second t-channel diagram. The spin effects in such decays were studied in [70].

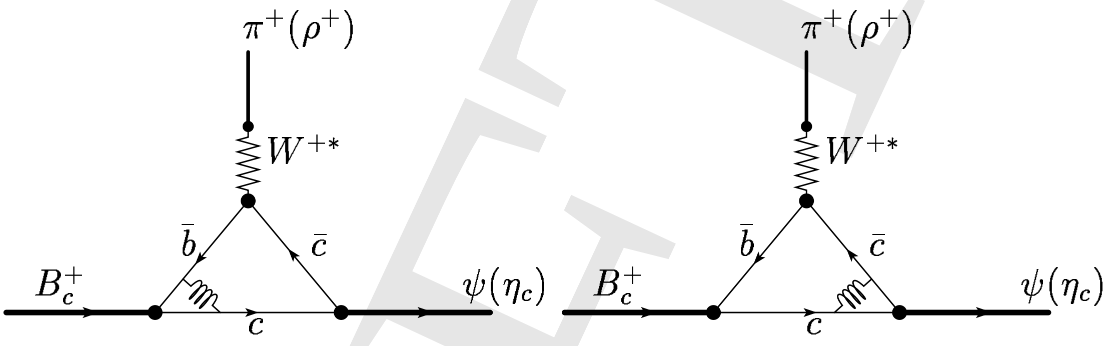

Figure 1.20: The diagrams of $B_c^+ \to \psi(\eta_c)\pi^+(\rho^+)$ decays with account for the hard gluon exchange between the constituents.

The relative yield of excited charmonium states can be also evaluated

$$\frac{\mathrm{BR}^{\mathrm{HS}}(B_c^+ \to \psi(2S)\pi^+)}{\mathrm{BR}^{\mathrm{HS}}(B_c^+ \to \psi\pi^+)} = \frac{\mathrm{BR}^{\mathrm{HS}}(B_c^+ \to \eta_c(2S)\pi^+)}{\mathrm{BR}^{\mathrm{HS}}(B_c^+ \to \eta_c\pi^+)} \approx 0.36. \tag{1.43}$$

Table 1.6: The widths of nonleptonic B_c decay modes and branching fractions calculated at $\tau_{B_c} = 0.46$ ps. We put a_1=1.26.

mode	BR, %
$\psi\pi^+$	0.67 ± 0.07
$\eta_c\pi^+$	0.87 ± 0.09
$\psi\rho^+$	1.96 ± 0.20
$\eta_c\rho^+$	2.43 ± 0.24

The suppressed decays caused by the flavor changing neutral currents was studied in [71].

The CP-violation in the B_c decays can be investigated in the same manner as made in the B decays. The expected CP-asymmetry of $\mathcal{A}(B_c^\pm \to J/\psi D^\pm)$ is about $4 \cdot 10^{-3}$, when the corresponding branching ratio is suppressed as 10^{-4} [72]. Thus, the direct study of CP-violation in the B_c decays is practically difficult because of low relative yield of B_c with respect to ordinary B mesons: $\sigma(B_c)/\sigma(B) \sim 10^{-3}$.

Another possibility is the lepton tagging of B_s in the $B_c^\pm \to B_s^{(*)} l^\pm \nu$ decays for the study of mixing and CP-violation in the B_s sector [73].

1.3.4.6 Discussion and Conclusions

We have reviewed the current status of theoretical predictions for the decays of B_c meson. We have found that the various approaches: OPE, Potential models and QCD sum rules, result in the close estimates, while the SR as explored for the various heavy quark systems, lead to a smaller uncertainty due to quite an accurate knowledge of the heavy quark masses. So, summarizing we expect that the dominant contribution to the B_c lifetime is given by the charmed quark decays ($\sim 70\%$), while the b-quark decays and the weak annihilation add about 20% and 10%, respectively. The coulomb-like α_s/v-corrections play an essential role in the determination of exclusive form factors in the QCD SR. The form factors obey the relations dictated by the spin symmetry of NRQCD and HQET with quite a good accuracy expected.

At the moment we certainly state that the accurate direct measurement of B_c lifetime can provide us with the information on both the masses of charmed and beauty quarks and the normalization point of non-leptonic weak lagrangian in the B_c decays (the a_1 and a_2 factors). The experimental study of semileptonic decays and the extraction of ratios for the form factors can test the spin symmetry derived in the NRQCD and HQET approaches and decrease the theoretical uncertainties in the corresponding theoretical evaluation of quark parameters as well as the hadronic matrix elements, determined by the nonperturbative effects caused by the quark confinement. The measurement of branching fractions for the semileptonic and non-leptonic modes and their ratios can inform on the values of factorization parameters, which depend again on the normalization of non-leptonic weak lagrangian. The charmed quark counting in the B_c decays is related to the overall contribution of b quark decays as well as with the suppression of $\bar{b} \to c\bar{c}\bar{s}$ transition because of the destructive Pauli interference, whose value depends on the nonperturbative parameters (roughly estimated, the leptonic constant).

Thus, the progress in the measuring the B_c lifetime and decays could enhance the theoretical understanding of what really happens in heavy quark decays.

1.3.5 DØ Study of B_c: Triggering and Reconstruction †

1.3.5.1 Introduction

The B_c meson is a particularly interesting system to study since it contains two different heavy quarks that are often in competition regarding subsequent decays. As a result, measurements of its properties such as mass, lifetime, and decay branching ratios offer a unique window into heavy quark hadrons. Since it has non-zero flavor, it has no strong or electromagnetic decay channels, and it is the last or heaviest such meson predicted by the Standard Model. Its weak decay is expected to yield a large branching fraction to final states containing a J/ψ which is a useful experimental signature. The B_c meson (as well as b baryons and double-heavy baryons) is too massive to produce at the B factories running at the $\Upsilon(4S)$. LEP has only a few B_c candidates, while CDF isolated a sample of 23 B_c

† Author: Rick Van Kooten

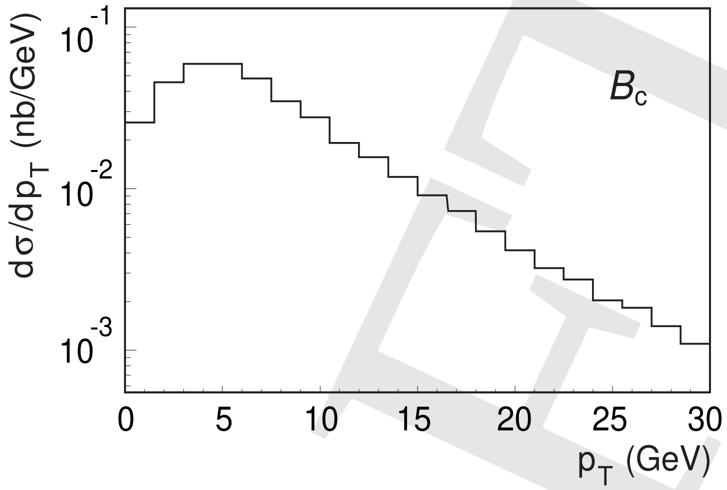

Figure 1.21: The differential B_c cross section used in the following studies.

decays in approximately 100 pb^{-1} of data [45] in Run I resulting in the prediction that $\sigma(B_c)/\sigma(b) \approx 2 \times 10^{-3}$.

1.3.5.2 DØ Simulations

To examine DØ prospects for Run II, simulations were made of B_c production using PYTHIA and reweighting the resulting spectrum to match the differential $d\sigma/dp_T$ cross section calculated using code supplied by the authors of Ref. [46]. After reweighting, the production spectrum of produced B_c mesons is shown in Fig. 1.21. The mass of the B_c meson was set to 6.40 GeV and the lifetime to 0.50 ps, consistent with CDF and LEP measurements [45,47]. The fraction of $b \to B_c$ was increased to 0.5 while the fractions of $b \to B_d^0$, B^+, B_s^0, and Λ_b were scaled down appropriately. Any events containing two B_c mesons were discarded in other to get the hadron composition of the "away-side" B hadron correct. Events with $p_T(B_c) > 3$ GeV and $|\eta(B_c)| < 3$ were retained.

The CLEO QQ package was used to force the semileptonic decay $B_c \to J/\psi\ell\nu$ (Br $\approx$ 2.5% [48]) and $B_c \to J/\psi\pi$ (Br $\approx$ 0.2% [48]) followed by the subsequent decays of $J/\psi \to e^+e^-$ or $J/\psi \to \mu^+\mu^-$. The distinctive trilepton signature of the first decay mode was used to allow efficient triggering from the presence of at least two electrons or muons with significant transverse momentum with reasonable background rates.

Detector simulations were performed at a number of different levels of sophistication: MCFAST [49], PMCS (a DØ parameterized fast Monte Carlo), and full GEANT simulated events to allow the use of a more realistic trigger simulator and reconstruction resolution determination. Typical distributions of B_c decay products from the MCFAST simulation are shown in Fig. 1.22.

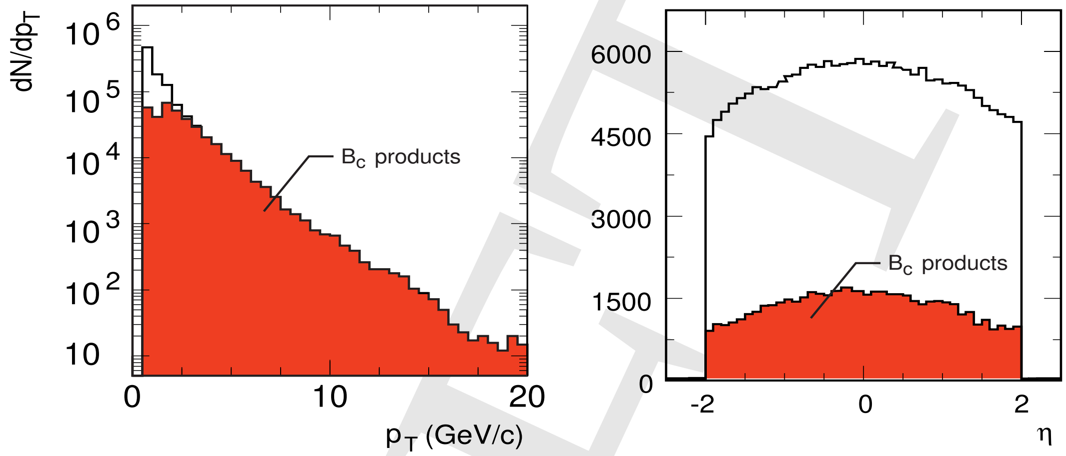

Figure 1.22: Kinematic distributions of B_c decay products (a) p_T and (b) η for the semileptonic decay.

1.3.5.3 Results

MCFAST simulations could be used to determine kinematic and trigger efficiencies; however, the DØ trigger simulator was run on GEANT fully simulated events for a more sophisticated and reliable treatment. Starting with the case of a semileptonically decaying B_c where all three leptons are muons, Table 1.7 gives the DØ muon trigger efficiency for the indicated criteria. "Medium" muon identification criteria refers to .... and "Tight" muon identification criteria refers to xxx.

The status of the simulation of triggering on electrons is less complete, and trigger efficiencies in this case were extrapolated from prior studies [50] for the decay $B_d^0 \to J/\psi K_S^0$. At Level 1, information from the electromagnetic calorimeter, the fiber tracker, and matches between these and hits in the central preshower detector are expected to lead to a trigger efficiency of approximately 30%, but with a substantial background rate. This background rate is expected to be lowered to a reasonably low value with invariant mass cuts on the electrons from the $J/\psi \to e^+e^-$ decay appplied at Level 2 of the trigger. An overall efficiency for triggering on states with di-electrons from the J/ψ decay is estimated to be 12.8%.

Although DØ will initially not be running with a vertex silicon track trigger, studies were made of the potential for such a trigger to benefit isolating a large sample of B_c mesons. Note that the events were generated with a B_c lifetime set to 0.50 ps rather than the usual lifetimes of 1.5–1.6 ps of the other B mesons. A decay length resolution of 116 μm has been measured in MCFAST simulated events. A vertex silicon track trigger would operate by examining the impact parameter signficance, i.e., b/σ_b, where b is the impact parameter of a track and σ_b its error. The distribution of this quantity for tracks from B_c decay is shown in Fig. 1.23(a). This distribution is substantially narrower than for tracks from other B meson decays due to the shorter lifetime of the B_c. The trigger efficiency obtained by cutting on the presence of one or more tracks with significantly large impact parameter is shown in Fig. 1.23(b). For the same background rate, the efficiency is about a factor of 2.5 times smaller than the comparable rate for $B_d^0 \to J/\psi K_S^0$ decays.

Criteria	Efficiency	DØ Designation
Single Muon $p_T^\mu > 4$ GeV $\lvert\eta^\mu\rvert < 1.5$ "Medium"	0.23	MTM5, MUO(1,4,A,M)
$p_T^\mu > 4$ GeV $\lvert\eta^\mu\rvert < 1.5$ "Tight"	0.08	MTM6, MUO(1,4,A,T)
Di-Muon Both $p_T^\mu > 2$ GeV $\lvert\eta^\mu\rvert < 1.5$ "Medium"	0.16	MTM10, MUO(2,2,A,M)
Both $p_T^\mu > 4$ GeV $\lvert\eta^\mu\rvert < 2.0$ "Medium"	0.15	MTM12, MUO(2,4,A,M)
"Or" of above	0.28	

Table 1.7: DØ Level 1 muon trigger efficiencies for trilepton final states from semileptonic decay of B_c mesons with $p_T(B_c) > 3$ GeV and $|\eta(B_c)| < 3$.

In the $B_c \to J/\psi \ell \nu$ channel, a typical ,mass reconstruction of the J/ψ through its decay into $\mu^+\mu^-$ is shown in Fig. 1.24(a) indicating a mass resolution σ_m of 29 MeV. Events are required to have the two leptons assigned to the J/ψ to have an invariant mass within $2\sigma_m$ of the J/ψ mass. To reduce backgrounds, the p_T of the combined (J/ψ plus lepton) system was requireed to be greater than 8 GeV, and the decay length of the J/ψ-lepton vertex was required to be greater than 50 μm. Kinematic quantities such as the trilepton invariant mass which yields infor- mation on the mass of the decaying state (Fig. 1.24).

Similar studies were extended to the $B_c \to J/\psi\pi$ decay channel that would allow an exclusive reconstruction of the B_c meson but with smaller statistics due to the small (0.2%) branching ratio for this final state. With only two leptons to trigger on, the overall trigger efficiency for the di-muon final state analogous to that shown in Table 1.7 with a slightly lower total trigger efficiency of 0.24. The mass resolution of the reconstructed B_c without constraints to the J/ψ mass is found to be 52 MeV.

To estimate the expected number of B_c events reconstructed by DØ in the 2 pb^{-1} of Run II, the estimate of $\sigma(B_c^+)/\sigma(\bar{b}) = 1.3 \times 10^{-3}$ compared to the measurement of $\sigma(B^+)/\sigma(\bar{b}) = 0.378 \pm 0.022$ could be used. It is more straightforward to use the CDF measurement [45] of

$$\frac{\sigma(B_c^+) \cdot \mathrm{B}r(B_c^+ \to J/\psi \ell \nu)}{\sigma(B^+) \cdot \mathrm{B}r(B^+ \to J/\psi K^+)}$$

and comparisons of DØ's trigger and reconstruction efficiency with corresponding CDF

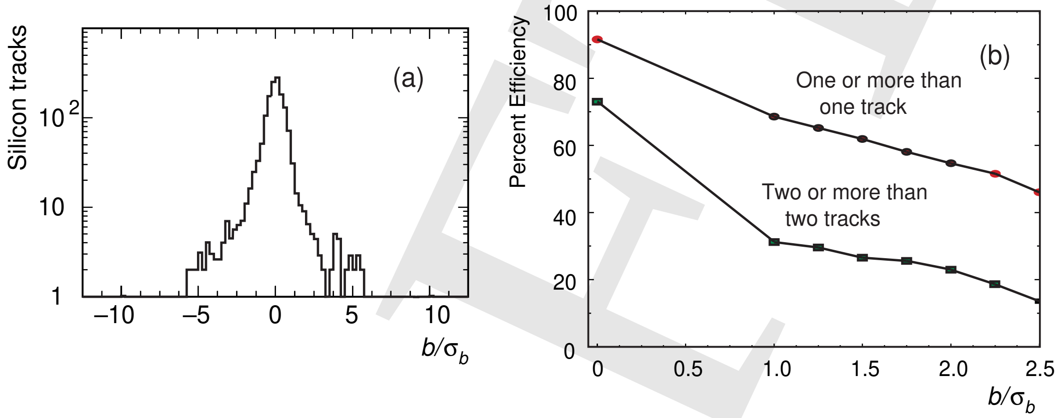

Figure 1.23: (a) Impact parameter divided by its error for track from $B_c \to J/\psi \ell \nu$; (b) efficiency of future silicon track trigger as a function of cut on b/σ_b.

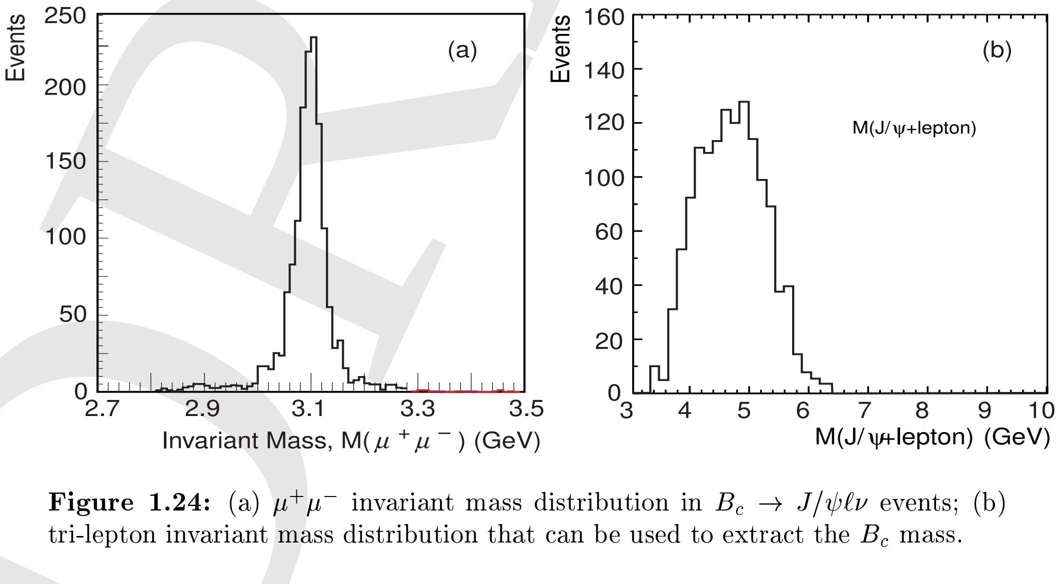

Figure 1.24: (a) $\mu^+\mu^-$ invariant mass distribution in $B_c \to J/\psi \ell \nu$ events; (b) tri-lepton invariant mass distribution that can be used to extract the B_c mass.

efficiencies. This leads to an estimate that approximately 600 fully reconstructed $B_c^+ \to J/\psi \ell \nu$ would be available after Run II, which is a large enough sample to make significant improvements in lifetime and mass measurements to increase our understanding of the B_c system. In addition, samples of 30–40 fully exclusive decays such as $B_c^+ \to J/\psi \pi$ can also be expected that would clearly supplement the semileptonic decay measurements which suffer from the escaping neutrino. Of course, proportionally much larger samples would be expected in subsequent runs of the Tevatron beyond Run IIa.

1.3.5.4 Double-Heavy Baryons

The investigation of properties of hadrons containing one or more heavy quarks is very important for understanding the dynamics of quark and gluon interactions. In addition to the study of the meson, double-heavy baryons include further information on spin dynamics in such a system.

We have studied the experimental prospects for isolating double-heavy baryons. Surprisingly, baryons containing either two charm quarks, two b quarks, or one of each quark are produced at respectable rates at the Tevatron as shown in Fig.1.17 where it is noted that the production rate for QQq is predicted to be as much as 50% of the production rate for B_c.

After examining production rates, decay diagrams involving spectator decays or W-exchange (including Cabbibo-suppressed decays) were considered. A new feature that was studied were decays of double-heavy baryons to 's which are favored decay modes because of ease of triggering and also because they absorb Q-value which would otherwise produce pion multiplicity contributing to combinatorial background. It is predicted that "golden" exclusive decay modes such as ?????or ????? into triggerable modes have small total branching ratios between ????? and ??????, although the inclusive rate for may be as high as ?????.

Final states containing J/ψ's may be the only modes accessible without a silicon vertex track trigger. Other final states that can possibly be cleanly reconstructed are those containing ???? or ????. A general signature for double-heavy baryon production of a displaced vertex containing a proton (or other baryon) is also important to consider.

Decays without a ψ may still be accessible due to cascading decays. A double-heavy baryon decaying into either a b-baryon or another Double-heavy baryon should present no problem since the decay lengths will give rise to a large number of high-impact parameter tracks that could allow the use of a vertex/silicon track trigger. A double-heavy baryon with a short lifetime (e.g., estimates of xx ps, xx ps, and xxps) can decay into a charm meson with a reasonably long lifetime such as the D????(ps). The large mass of the double-heavy baryon parent can give substantial transverse momentum kick with respect to the original flight direction. Including a fairly long charm decay length, the final decay products can have impact parameters comparable to those of b hadrons (see simulation results of Fig. 2-8(b)) and possibly reasonable efficiency for a vertex/silicon track trigger.

Figure 1.25: Figure 1-2 (a) Production cross section as a function of minimum xx for double-heavy baryons compared with the production of mesons; (b) impact parameter distribution of decay products of double-heavy baryons with a cascade through charm compared to distributions of xx and yyy.

1.3.6 Looking for Ξ_{bc}-Baryons†

1.3.6.1 Decays of DHB

The lifetime for the ground states of DHB has been calculated in the framework of Operator Product Expansion (OPE) and expansion over inverse heavy quark mass [55]. In leading order of OPE the inclusive widths are determined by the spectator mechanism with QCD-correction. The next order in the OPE allows us to take into account the corrections connected with the quark motion in the DHB and with the chromomagnetic quark interaction. The Pauli interference (PI) between initial and final states as well as the weak scattering (WS) play important role in the mechanism of DHB-baryon decay. For example, PI leads to the increase of the b-quark decay contribution to bc-baryon by the factor of 2. Overall effect of the corrections to the spectator mechanism can achieve $40 \div 50\%$. In Tables I and II we show the contributions of the different modes to the total decay widths of doubly charmed and bc-baryons. One can see from these Tables, that the WS contributions are comparable with spectator ones, and we will use this fact in further estimates.

Table I.

Mode	width, ps^{-1}	contribution, % for Ξ_{cc}^{++}	contribution, % for Ξ_{cc}^{+}
$c \to sdu$	2.894	124	32
$c \to se^+\nu$	0.380	16	4
PI	-1.317	-56	-
WS	5.254	-	559

The following estimates of the lifetime were done for Ξ_{cc}-and Ξ_{bc}-baryons [5]

$$\begin{aligned} \tau_{\Xi_{cc}^{++}} &= 0.43 \pm 0.1\ ps \\ \tau_{\Xi_{cc}^{+}} &= 0.12 \pm 0.1\ ps \\ \tau_{\Xi_{bc}^{+}} &= 0.33 \pm 0.08\ ps \\ \tau_{\Xi_{cc}^{0}} &= 0.28 \pm 0.07\ ps \end{aligned}$$

Let us consider, first, the spectator decay modes. In the Table 3 we give some examples of the exclusive (spectator) decay modes of DHB calculated in the framework of QCD sum

†Author: A. Likhoded

rules [56]. As one can see, some of decay modes have surprisingly large branching fractions: $\Xi_{cc}^{+} \to \Xi_{cs}^{0}\pi^{+}(\rho^{+})$, $\Xi_{cc}^{++} \to \Xi_{cs}^{+}\pi^{+}(\rho^{+})$ and semileptonic ones. However, the spectator decays lead to the cascade of consequent decays, and to two or three secondary vertices in the experiment, and the analysis of such events seems to be quite cumbersome.

We want to consider another possibility. As it was shown above, the contribution of WS

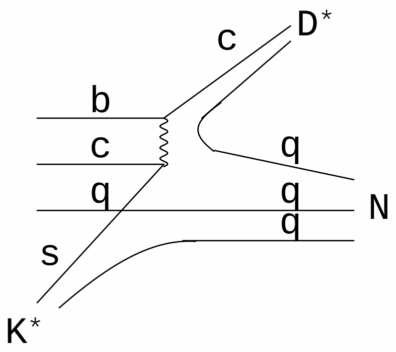

Figure 1.26: *bcq* baryon decay

to the Ξ_{bc}^{+} and Ξ_{bc}^{0} decays is about 20%. This type of decay (see Fig. 1.26) is characterized by specific kinematics: in the rest frame of Ξ_{bc}-baryon the c- and s-quarks move in the opposite directions with the high momentum value of about 3.2 GeV. Both c- and s-quarks then fragment producing multiparticle final states.

Let us estimate in this case the probability of a configuration which is close to the following exclusive limit:

$$\Xi_{bc} \to D^{(*)}K^{(*)}N$$

To do this it is necessary to produce $D^{(*)}$ and $K^{(*)}$ by fragmentation processes: $c \to D^{(*)} + X_q$ and $s \to K^{(*)} + X_q$ in the hard part of fragmentation spectrum with $z > 0.8$ and $X_q \sim q$. Here, light quark q has a small momentum $p_q \sim 0.6$ GeV.

Using the well-known parametrization for fragmentation functions one gets:

$$Br(\Xi_{bc} \to D^{(*)}K^{(*)}N) = Br(WS) \cdot W(z_D > 0.8) \cdot W(z_K > 0.8)$$
$$Br(\Xi_{bc} \to D^{(*)}K^{(*)}N) = 0.2 \cdot 0.2 \cdot 0.04$$

So, we can have the probability of Ξ_{bc}-decay exclusive mode $D^{(*)}K^{(*)}N$ to be equal to 0.16%, and if our estimates are not far from reality, we have to expect

$$N_{\Xi_{bc}} \approx 10^5 \cdot 1.5 \cdot 10^{-3} \sim 150 \text{ events}$$

Of course, the detection efficiency could reduce this number, but the increase of the integrated luminosity allows us to hope that the observation of Ξ_{bc} will be coming soon.

Table II.

Mode	contribution, % for Ξ_{bc}^{+}	contribution, % for Ξ_{bc}^{0}
$b \to c + X$	20	17
$c \to s + X$	37	31
PI	23	20
WS	20	31

Table III.

Mode	Br (%)	Mode	Br (%)
$\Xi_{bb}^{\diamond} \to \Xi_{bc}^{\diamond} l \bar{\nu}_l$	11.2	$\Xi_{bc}^{+} \to \Xi_{cc}^{++} l \bar{\nu}_l$	3.5
$\Xi_{bc}^{0} \to \Xi_{cc}^{+} l \bar{\nu}_l$	3.3	$\Xi_{bc}^{+} \to \Xi_{bs}^{0} \bar{l} \nu_l$	3.0
$\Xi_{bc}^{0} \to \Xi_{bs}^{-} \bar{l} \nu_l$	2.8	$\Xi_{cc}^{++} \to \Xi_{cs}^{+} \bar{l} \nu_l$	14.9
$\Xi_{cc}^{+} \to \Xi_{cs}^{0} \bar{l} \nu_l$	6.9	$\Xi_{bb}^{\diamond} \to \Xi_{bc}^{\diamond} \pi^{-}$	0.3
$\Xi_{bb}^{\diamond} \to \Xi_{bc}^{\diamond} \rho^{-}$	3.4	$\Xi_{bc}^{+} \to \Xi_{cc}^{++} \pi^{-}$	0.6
$\Xi_{bc}^{0} \to \Xi_{cc}^{+} \pi^{-}$	0.55	$\Xi_{bc}^{+} \to \Xi_{cc}^{++} \rho^{-}$	1.5
$\Xi_{bc}^{0} \to \Xi_{cc}^{+} \rho^{-}$	1.4	$\Xi_{bc}^{+} \to \Xi_{bs}^{0} \pi^{+}$	13.1
$\Xi_{bc}^{0} \to \Xi_{bs}^{-} \pi^{+}$	12.3	$\Xi_{bc}^{+} \to \Xi_{bs}^{0} \rho^{+}$	5.6
$\Xi_{bc}^{0} \to \Xi_{bs}^{-} \rho^{+}$	5.2	$\Xi_{cc}^{++} \to \Xi_{cs}^{+} \pi^{+}$	8.1
$\Xi_{cc}^{+} \to \Xi_{cs}^{0} \pi^{+}$	4.2	$\Xi_{cc}^{++} \to \Xi_{cs}^{+} \rho^{+}$	45.1
$\Xi_{cc}^{+} \to \Xi_{cs}^{0} \rho^{+}$	24.8		

State	Lifetime $[ps]$	Mass[GeV]	Interesting Decay modes
$\Xi_{cc}^{++}(ucc)$	0.43 [39]	3640 [42]	
$\Xi_{cc}^{+}(dcc)$	0.11 [39]	3640 [42]	
$\Omega_{cc}^{+}(scc)$	0.5 [42]	3800 [42]	
$\Omega_{ccc}^{++}(ccc)$	0.3 [42]	4925 [42]	
$\Xi_{cb}^{+}(ucb)$	0.33 ± 0.08 [38]	3650	
$\Xi_{cb}^{0}(dcb)$	0.28 ± 0.07 [38]	3650	
$\Omega_{cb}^{0}(scb)$	xxx []	7.120 []	
$\Xi_{cbc}^{+}(ccb)$	xx []	3650 []	
$\Xi_{bb}^{0}(ubb)$	0.79 [40]	10.250 []	
$\Xi_{bb}^{-}(dbb)$	0.8 [40]	10.250 []	
$\Omega_{bb}^{-}(sbb)$	0.8 [40]	10.395 []	
$\Xi_{bbc}^{0}(bbc)$	$0.xx$ []	11.48 [41]	
$\Omega_{bbb}^{-}(bbb)$	$0.xx$ []	14.76 [41]	

1.4 Fragmentation[†]

1.4.1 Introduction

Our understanding of how quarks and gluons fragment into hadrons is now quite mature. In single particle inclusive processes described by perturbative QCD, this process is factorized (up to power-suppressed corrections) from the hard interaction and encoded in a non-perturbative fragmentation function (FF) $D_i^H(x,\mu)$: the probability density of H in parton i with momentum fraction x at factorization scale μ. In general, as with initial state parton distribution functions (PDF's) this fragmentation function is not calculable, in contrast to its evolution with μ (which is due to radiation of the fragmenting parton). The evolution equation for FF's is identical in form to the DGLAP evolution equation for PDF's, although the evolution kernels differ from two loop onwards. Although non-perturbative, these FF's are universal so that they may be determined for each hadron H in a few calibration experiments at some fixed scale μ_0, for use in other experiments and at other values of μ. See e.g. [74].

The fragmentation of heavy quarks [4] is different. At energies E of the order of the heavy quark mass m one must only account for the non-perturbative transition of the heavy quark to the hadron of interest, which one assumes describable by a non-perturbative FF. One may take the point of view that one should just parametrize this function with a polynomial ansatz e.g. and let data determine its form. Or, one may let physical considerations inspire the functional form. The most famous form in the latter philosophy is the Peterson et al. [75] model. More recent forms, based on heavy quark effective field theory, are described

[†]G. Bodwin, R. Field, B. Harris, R. van Kooten, E. Laenen, S. Menary, E. Norrbin, C. Oleari

[4]Charm and bottom: top decays by the weak interaction before fragmentation sets in.

in section 1.5.

At energies or scales much larger than the heavy quark mass, one must account for large logarithms $\ln(E/m)$ to all orders, in order to use perturbation with confidence. This may be done using perturbative FF's (PFF's). They are perturbative because the coupling constant is small enough in the scale range from m to E on the one hand, and on the other because the mass screens the collinear divergences which plague massless-quark fragmentation and require the non-perturbative FF's to absorb them. The perturbative and non-perturbative FF's must of course be matched together to enable a confrontation with data.

Heavy quark FF's are special for another reason. Perturbative calculations show that there is in general a high probability that an observed energetic heavy-flavored hadron (e.g. a B- or D-mesons) is a fragment of a produced hard heavy quark. Thus, the tagging of heavy quark flavored hadrons provides a direct window to quark-gluon dynamics.

Our understanding of the perturbative stage of heavy quark fragmentation has matured substantially in the past decade. From the observation that a large part of the heavy quark fragmentation process could be described perturbatively, Mele and Nason [76] computed the initial condition to the evolution equation for the heavy quark FF in perturbation theory to next-to-leading order. [More history..]

Outside the context of factorization-based perturbative QCD, there is the quite successful string model of the Lund group. We shall encounter this approach in more detail when discussing possible beam drag effects in section 1.6.

Yet other approaches to heavy quark fragmentation exist [BKL], but for lack of space and time we shall not discuss them here. We refer to the recent LHC report [77] for more studies on heavy quark fragmentation.

In the following we begin with discussing perturbative fragmentation and describe an attempt to learn more about the non-perturbative FF from the very precise SLD data. Then the theory of the non-perturbative FF is reviewed and clarified. Next we discuss the phenomenon of beam drag as (perhaps) observed at HERA in charm DIS and photoproduction, and present a study of the possible impact of this effect on CDF/D0 and BTeV studies. We also discuss various other "systematic errors" in heavy quark FF's, in section 1.7.

1.4.2 Perturbative Fragmentation

A well-defined fragmentation function is a universal function, so that its study can be undertaken in the context of e^+e^- collisions without the complication due to initial state hadrons. We are interested in the situation where the typical scale E of the process is much larger than the heavy quark mass m, a typical situation at the Tevatron. As mentioned above, this means one must resum large logarithms $\ln(E/m)$ to all orders in the hard scattering cross section, for the computation of a reliable differential cross section. This is achieved by the formalism of the perturbative FF (PFF), briefly as follows. The PFF satisfies the DGLAP [78–80] evolution equation:

$$\frac{dD_{i,\mathrm{pert}}(x,\mu)}{d\ln\mu} = \sum_j \int_x^1 \frac{dz}{z} P_{ij}(\frac{x}{z}, \alpha_s(\mu)) D_{j,\mathrm{pert}}(z,\mu)\,, \tag{1.44}$$

where i,j label parton flavors. With an initial condition at $\mu_0 \simeq m$, (1.44) determines the PFF at x,μ, and resums $\ln(\mu/\mu_0)$ to all orders. This initial condition for the PFF was first computed in [76] and is, for $i = Q$

$$D_{Q,\mathrm{pert}}(z,\mu_0) = \delta(1-z) + \frac{\alpha_s(\mu_0)C_F}{2\pi}\left[\left(\frac{1+z^2}{1-z}\right)\left(\ln(\frac{\mu_0^2}{m^2}) - 1 - 2\ln(1-z)\right)\right]_+ . \tag{1.45}$$

For heavy quark production at $E \gg m$, the choice $\mu = E$ in the solution of (1.44) then resums the $\ln(E/m)$ logarithms to all orders in α_s and to next-to-leading logarithmic (NLL) accuracy.

To study the PFF in the context of e^+e^- collisions, one may factorize the single heavy *quark* inclusive cross section as

$$\frac{d\sigma}{dx}(x,E,m) = \sum_i \int_x^1 \frac{dz}{z}\frac{d\hat\sigma_i}{dz}(z,E,\mu_F)\; D_{i,\mathrm{pert}}\left(\frac{x}{z},\mu_F,m\right)\,, \tag{1.46}$$

where $d\hat\sigma_i(x,E,\mu_F)/dx$ are the (scheme- and process-dependent) partonic cross sections for producing the parton i, and $D_{i,\mathrm{pert}}(x,\mu_F,m)$ are the (scheme- but not process-dependent) perturbative fragmentation functions (PFF's) for parton i to evolve into the heavy quark Q. The factorization scale μ_F must be chosen of order E, to avoid the appearance of large logarithms of E/μ_F in the partonic cross sections.

Note that for heavy-quark production in hadronic collisions at $p_T \gg m$, it is customary to choose $E \sim p_T$, while in e^+e^- collisions E is the centre-of-mass energy.

The single-*hadron* inclusive cross section, including non-perturbative corrections, is then written as multiple convolution

$$\frac{d\sigma^H}{dx}(x,E,m) = \sum_i \frac{d\hat\sigma_i}{dx}(x,E,\mu_F) \otimes D_{i,\mathrm{pert}}(x,\mu_F,m) \otimes D^H_{\mathrm{NP}}(x)\,. \tag{1.47}$$

i.e. the full fragmentation function requires combining the perturbative FF with a non-perturbative part modeling the final hadronization.

The weak point of Eq. (1.46) comes from this initial condition which is computed as a power expansion in terms of $\alpha_s(m)$. In particular, irreducible, non-perturbative uncertainties of order Λ_{QCD}/m are present. We assume that all these effects are described by a non-perturbative fragmentation function D^H_{NP}, that takes into account all low-energy effects, including the process of the heavy quark turning into a heavy-flavored hadron H. There are theoretical approaches to the fragmentation-function calculation that rely upon heavy-quark effective theory in order to study more systematically non-perturbative effects [81,82]. These will be discussed in the next subsection. Here we want to establish a connection with the most commonly used parametrizations, and thus we will use the Peterson form and the "Euler" form $x^\alpha(1-x)^\beta$.

Let us first very briefly review the present situation. Heavy flavor production in e^+e^- collisions has been thoroughly studied both at fixed order [83–85] and in a combined fixed order plus next-to-leading logarithmic (here $\ln(E/m)$ with E the beam energy) resummed approach [86], using the Peterson function for the non-perturbative transition. [5] Increasing the order in perturbation theory turns out [86] to reduce the Peterson parameter ϵ, which corresponds to a harder non-perturbative fragmentation function. The importance of $\mathcal{O}(m/E)$ terms in the fixed-order part of the calculation is found to be minor.

The results [86] can be summarized as follows:

- increasing the order of the perturbative expansion and using a next-to-leading log (NLL) resummed approach turns out to reduce the Peterson parameter ϵ, which corresponds to a harder non-perturbative fragmentation function.

- The differential cross section obtained with a matching between the α_s^2 fixed order and the NLL resummed one, called the NLL improved, is harder than the NLL, so that the ϵ parameter needed in the non-perturbative part is, in general, slightly bigger than in the NLL case.

- At LEP energies, the importance of $\mathcal{O}(m/E)$ terms is found to be minor.

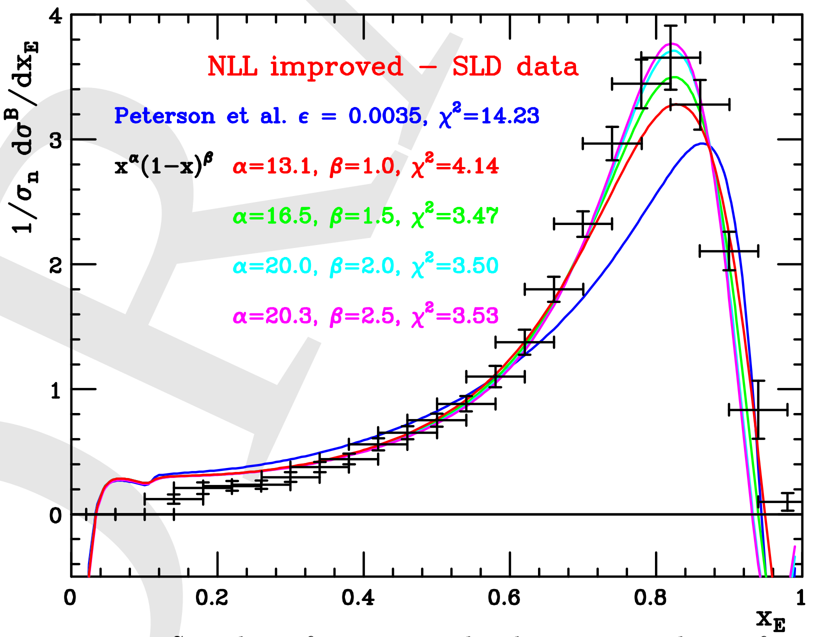

Figure 1.27: Fit to SLD data of Peterson and Euler non-perturbative fragmentation function via NLL improved calculation.

[5]This combined approach is actually a variable flavor number scheme (VFNS) for heavy quark fragmentation.

Here we show some new results obtained from a fit to SLD [92] B-production data in e^+e^- collision at $E = 91.2$ GeV are presented in Fig. 1.27. We have used two family of non-perturbative FF: the Peterson form and the Euler form $x^\alpha(1-x)^\beta$. We have fitted the data by χ^2 minimization, keeping $\Lambda^{(5)}_{\rm QCD}$ fixed to 200 MeV. With this procedure we have fitted both the value of ϵ and the normalization (which was allowed to float) for the Peterson, and the value of α and the normalization for the Euler form, varying β in the range between 1.0 and 2.5, with an incrementing step of 0.5.

We should caution at this point that the values of ϵ for the Peterson FF fitted above cannot be used for LEP studies, as the SLD and LEP collaborations use different values for some key input parameters such as what fraction of b quarks produces B^{**} mesons.

The Peterson form turns out to have a very poor χ^2/dof. For a comparison, in Fig. 1.28 we plot the non-perturbative FF at their best χ^2/dof values.

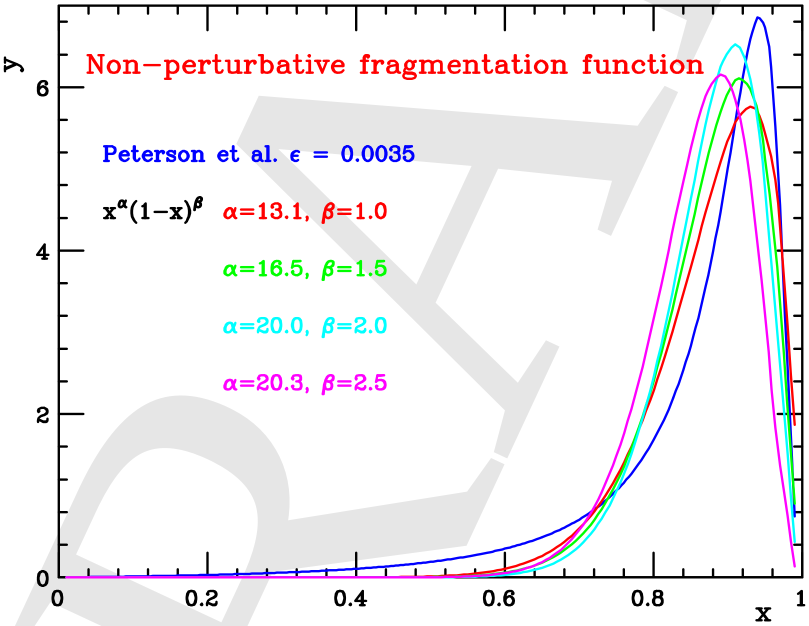

Figure 1.28: Functional forms of the non-perturbative fragmentation functions that produced the best fit to SLD data.

We note that in Ref. [87], and more recently in [88], the formalism used in the previous analysis of e^+e^- collisions has been applied to the Tevatron b-quark p_T cross section, for which the data exceed the central NLO-theory estimate by a factor of two. At large p_T the theoretical uncertainty due to scale variations was found to be reduced with respect to the fixed-order approach, but the cross section decreased. At moderate p_T, the cross section gets somewhat enhanced, but not enough to explain the data-theory discrepancy. Another study involving FF's in heavy-quark hadroproduction, in the context of the so-called ACOT VFNS, was performed in [89]. The PFF formalism was also applied to γp [90] and $\gamma\gamma$ [91] charm production. Similar conclusions were reached as for $p\bar{p}$ b-quark production.

1.5 Non-perturbative fragmentation

In this subsection we review the theory of the nonperturbative transition of a heavy quark into a heavy meson.

First, we examine the model of Peterson *et al.* [75] for a fast-moving heavy quark Q with mass m_Q to fragment into a heavy hadron H (consisting of $Q\overline{q}$) with mass m_H and a light quark q with mass m_q. The basic assumption in this model is that the amplitude for the fragmentation is proportional to $1/(\Delta E)$, where $\Delta E = E_H + E_q - E_Q$ is the energy denominator for the process in old-fashioned perturbation theory. It follows that the probability for the transition $Q \to H + q$ is proportional to $1/(\Delta E)^2$. Taking the heavy quark's momentum to define the longitudinal axis, one can express ΔE in terms of the magnitude of the heavy quark's momentum P_Q, the fraction z of the heavy quark's momentum that is carried by the heavy hadron, and the transverse momentum $p_\perp$ of the heavy hadron or the light quark:

$$\begin{aligned}
\Delta E &= \sqrt{m_H^2 + p_\perp^2 + z^2 P_Q^2} + \sqrt{m_q^2 + p_\perp^2 + (1-z)^2 P_Q^2} - \sqrt{m_Q^2 + P_Q^2} \\
&\approx \frac{m_H^2 + p_\perp^2}{2zP_Q} + \frac{m_q^2 + p_\perp^2}{2(1-z)P_Q} - \frac{m_Q^2}{2P_Q} + \cdots \\
&\approx -\frac{m_Q^2}{2P_Q}[1 - 1/z - \epsilon^2/(1-z)].
\end{aligned} \tag{1.48}$$

In the last line, we have set $m_H \approx m_Q$ and neglected $p_\perp^2$ relative to m_Q^2. In order to facilitate the comparison with heavy-quark effective theory below, we have chosen the definition $\epsilon \equiv 1 - m_Q/m_H \approx (m_q^2 + p_\perp^2)^{1/2}/m_Q$. (In Ref. [75], the definition $\epsilon_Q \approx (m_q^2 + p_\perp^2)/m_Q^2$ was taken.) Multiplying $1/(\Delta E)^2$ by a factor $1/z$ for the longitudinal phase space, one arrives at the following *ansatz* for the fragmentation function [75]:

$$D_Q^H(z) = \frac{N}{z[1 - 1/z - \epsilon^2/(1-z)]^2}, \tag{1.49}$$

where the normalization N is fixed by the condition

$$\sum_H \int dz D_Q^H(z) = 1, \tag{1.50}$$

and the sum extends over all hadrons that contain Q. Contrary to the claims in Ref. [75], we find that $D_Q^H(z)$ has a maximum at $z \approx 1 - \epsilon$ and a width of order ϵ.

Next we discuss the work of Jaffe and Randall [82], which provides a QCD-based interpretation of heavy-quark fragmentation in terms of the heavy-quark mass expansion. One begins with the standard Collins-Soper [93] definition of the fragmentation function for a heavy quark into a heavy hadron:

$$\hat{f}(z,\mu^2) = \frac{z}{4\pi}\int d\lambda e^{i\lambda/z}\frac{1}{2N_c}\mathrm{Tr}\, \not{n} \langle 0| h(\lambda n) |H'(P)\rangle \langle H'(P)| \overline{h}(0) |0\rangle\,, \tag{1.51}$$

where the trace is over color and Dirac indices, N_c is the number of colors, $h(x)$ is the heavy-quark field at space-time position x, P is the four-momentum of the heavy hadron, and n is defined by $n^2 = 0$ and $n \cdot p = 1$. The state $|H'(P)\rangle$ consists of the heavy hadron plus any number of additional hadrons. The matrix element is understood to be evaluated in the light-cone gauge $n \cdot A = 0$. We note that the definition (1.51) contains a factor z relative to the definition of the fragmentation function used in Ref. [82]. This factor z will be important in comparing with the work of Braaten *et al.* below.

Following the standard method for obtaining the heavy-quark-mass expansion, one decomposes the field $h(x)$ into the sum of large $h_v(x)$ and small $\underline{h}_v(x)$ components:

$$h_v(x) = e^{-im_Q v\cdot x} P_+ h(x) \tag{1.52}$$

$$\underline{h}_v(x) = e^{-im_Q v\cdot x} P_- h(x), \tag{1.53}$$

with $P_\pm = (1 \pm \not{v})/2$ and v the hadron's four velocity. The leading term in the mass expansion of $f(x, \mu^2)$ is contained in the large-large combination of fields:

$$\hat{f}(z,\mu^2) = \frac{z}{4\pi}\int d\lambda e^{i\lambda/z}\frac{1}{2N_c}\mathrm{Tr}\,\not{n} \\ \times \langle 0|\, P_+ h(\lambda n)\, |H'(P)\rangle \langle H'(P)|\, \overline{P_+ h(0)}\, |0\rangle\, e^{-im_Q \lambda n\cdot v} + \ldots\ . \tag{1.54}$$

In Ref. [82], it is argued that the matrix element in Eq. (1.54) is a dimensionless function $\mathcal{F}(\lambda\epsilon)$. This function may be written in terms of its Fourier transform:

$$\mathcal{F}(\lambda\epsilon) = 2\int_{-\infty}^{\infty} d\alpha e^{-i\alpha\lambda\epsilon} a(\alpha)\ . \tag{1.55}$$

Inserting Eq. (1.55) into Eq. (1.54), one can evaluate the integral, with the result

$$\hat{f}(z,\mu^2) = \frac{z}{\epsilon}\hat{a}\left(\frac{1/z - m_Q/m_H}{\epsilon}\right) + \ldots\ . \tag{1.56}$$

A more complete analysis in Ref. [82] also yields the next-to-leading term in the hadron mass expansion:

$$\hat{f}(z,\mu^2) = z\left[\frac{1}{\epsilon}\hat{a}(y) + \hat{b}(y) + \cdots\right] \tag{1.57}$$

where $y = (1/z - m_Q/m_H)/\epsilon$. The analysis in Ref. [82] does not yield a precise prediction for the functional form of a and b, but some general properties may be deduced. The function a describes, in the limit of infinite heavy-quark mass, the effects of binding in the heavy hadron on the heavy-quark momentum distribution. For a free heavy quark, $a(y)$ would be a δ-function at $y = 1$. In a heavy hadron, the binding smears the heavy-quark momentum distribution. It can be shown [82] that the distribution has a maximum at $z \approx 1 - \epsilon$ and a width of order ϵ. We find the Peterson *et al.* model described above to be in agreement with these results.

Braaten *et al.* [81] present a QCD-inspired model for the fragmentation of a heavy-quark into an $S-$wave light-heavy meson. In this model, the fragmentation function is computed in perturbative QCD (Born level) in an expansion in inverse powers of the heavy-quark mass. For the the projection of the Qq state onto the meson, Braaten *et al.* take the standard nonrelativistic-bound-state expression. For example, in the case of of a ${}^1S_0$ meson, they assume the Feynman rule for the QqH vertex to be

$$\frac{\delta_{ij}}{\sqrt{3}} \frac{R(0)\sqrt{m_H}}{\sqrt{4\pi}} \gamma_5 (1 + \not{v})/2, \tag{1.58}$$

where $R(0)$ is the radial wave function at the origin. Braaten *et al.* make use of a definition of the fragmentation function that is equivalent to the Collins-Soper definition (1.51). From the terms of leading order in the heavy-quark mass expansion, they obtain, in the case of a ${}^1S_0$ meson,

$$\hat{f} \approx N \left[\frac{1}{\epsilon} \frac{(1-y)^2}{y^6} (3y^2 + 4y + 8) - \frac{(1-y)^3}{y^6} (3y^2 + 4y + 8) \right], \tag{1.59}$$

where $N = 2\alpha_s^2 |R(0)|^2/(81\pi m_q^3)$. At first glance, this result may seem to contradict the Jaffe-Randall analysis, which shows that the terms of leading order in the heavy-quark mass expansion give a contribution that is contained entirely in the function $a(y)$ in Eq. (1.57). However, the factor z in the definition of the fragmentation function (1.51) is crucial here. From the definitions of y and ϵ, we have $z = 1/[1 - \epsilon(1-y)]$, and, so, we can re-write Eq. (1.59) as

$$\hat{f}/z \approx \frac{N}{\epsilon} \frac{(1-y)^2}{y^6} (3y^2 + 4y + 8), \tag{1.60}$$

which is of the form of $a(y)$ in Eq. (1.57).

There are several additional studies of the of the perturbative-QCD fragmentation function in the limit of a large heavy-quark mass. See Ref. [81] for references.

1.6 Beam drag

A puzzling situation has arisen in charm electroproduction and photoproduction at HERA. The data are well-described by NLO QCD plus Peterson fragmentation, except at low p_T and large rapidity It is surmised that remnant-beam drag effects, which have been modelled in the string fragmentation model [94], may exert influence here. It is important to understand this effect, as it affects $B - \bar{B}$ asymmetries at e.g. HERA-B [95], and thus CP violation measurements. An open problem is how to match the string model for beam drag to leading twist QCD.

[A bit of text on string fragmentation]

Figs. 1.29 to 1.32 are from Emanuel Norrbin.

1.7 Other issues

In this section we exhibit some of ambiguities occurring in the practical use of heavy quark fragmentation functions that have no definite theoretical resolution.

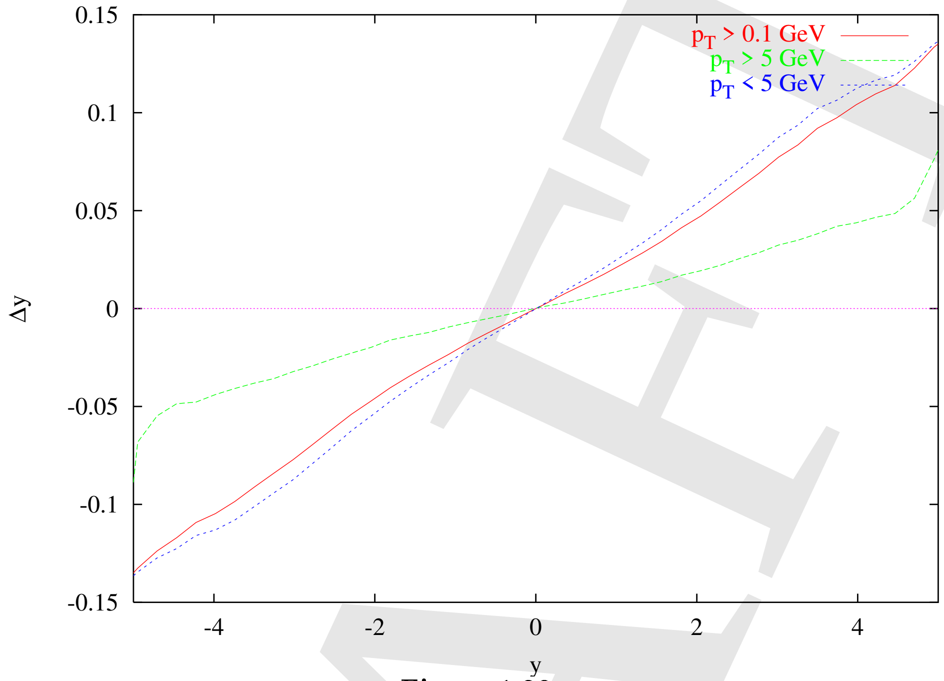

Figure 1.29:
Asymmetries due to beam drag from Pythia for 2 TeV $p\bar{p}$ collider.

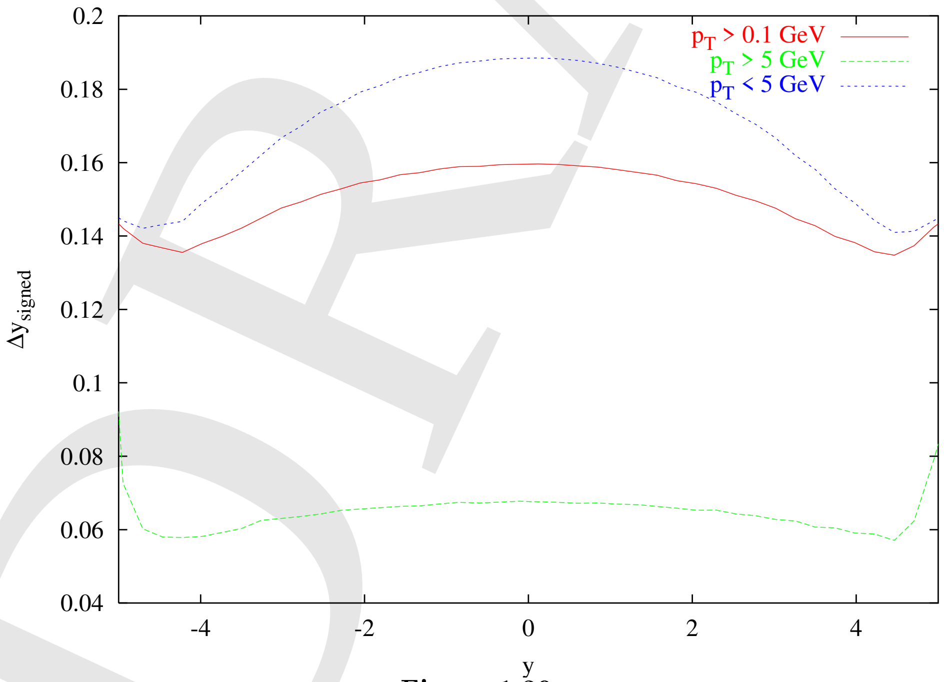

Figure 1.30:
Asymmetries due to beam drag from Pythia for 2 TeV $p\bar{p}$ collider.

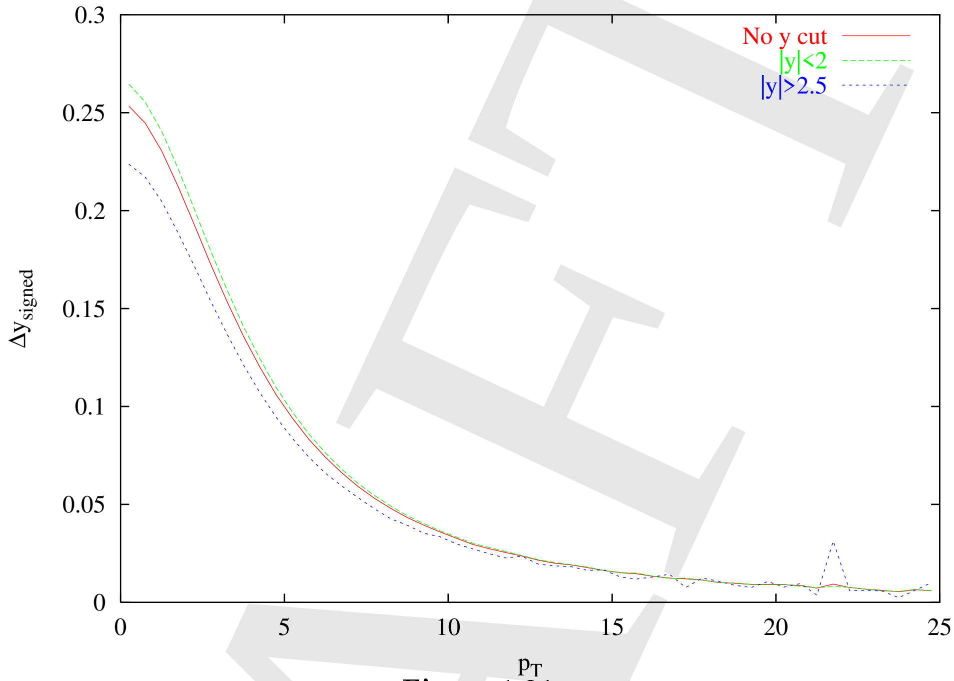

Figure 1.31:
Asymmetries due to beam drag from Pythia for 2 TeV $p\bar{p}$ collider.

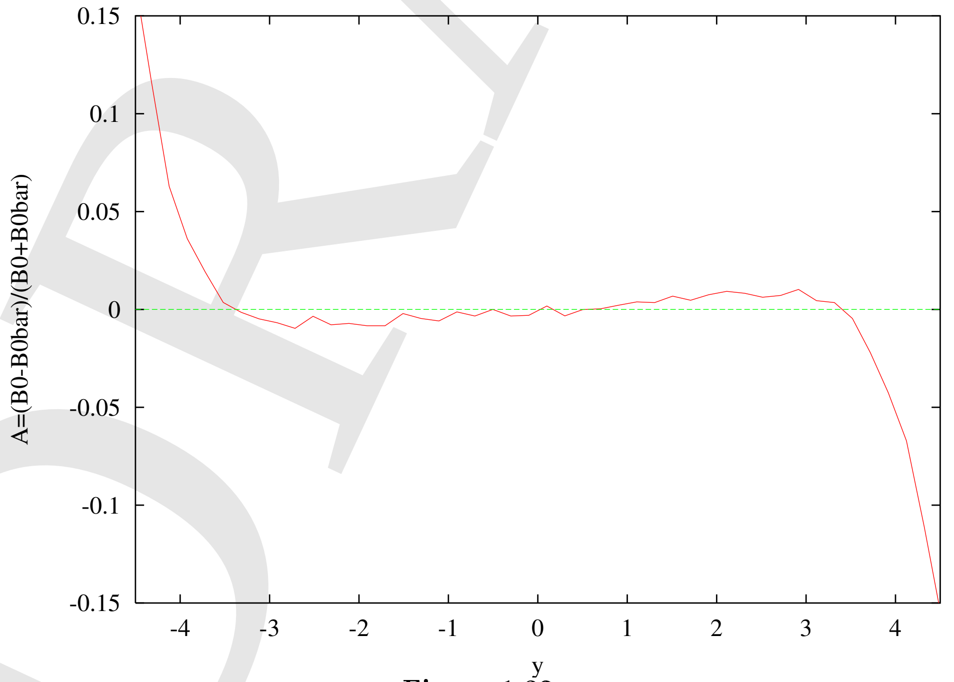

Figure 1.32:
Asymmetries due to beam drag from Pythia for 2 TeV $p\bar{p}$ collider.

1.7.1 Order of boosting and fragmenting

For example, when fragmenting a heavy quark to a heavy hadron there are various ambiguities, besides the choice of $\phi's$ and D:

- Shoud one use $\vec{p}_H = z\vec{p}_Q$ or $(E + p_{||})_H = z(E + p_{||})_Q$ or even something else?
- In a Monte Carlo program should one fragment in the lab frame or the parton cms frame?
- What is the interplay of such ambiguities with acceptance cuts?

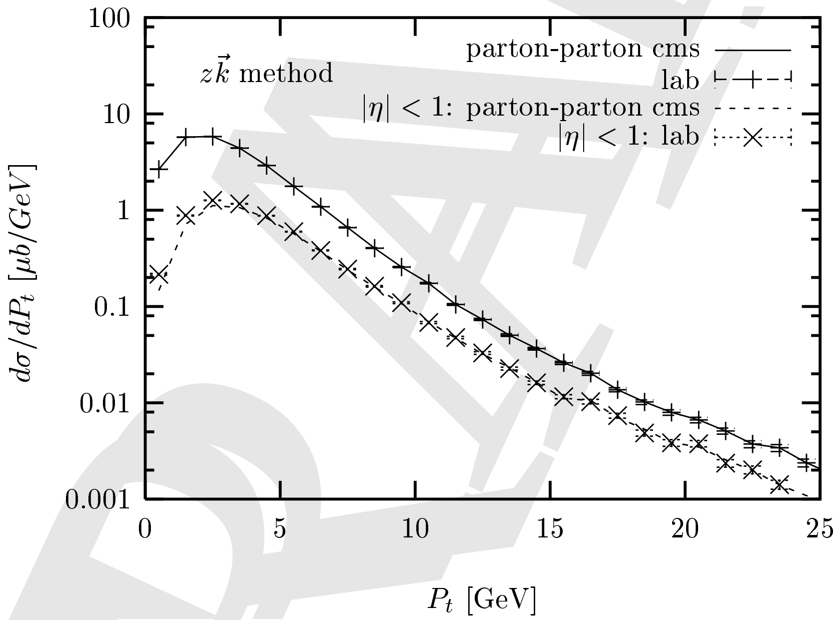

Figure 1.33:
Commutativity of boosting and fragmenting for P_T distribution.

In Fig. 1.33- 1.35 and table 1.7.1 we see that $\left[\text{boosting,fragment}\right] \neq 0$, but not too large for Tevatron B-production. We also note some interference with acceptance in particular at low p_T. In Figs. 1.36 we see noticeable dependence on the fragmentation "scheme" $(zp^\mu, z\vec{p}, zp^+)$, again at low p_T.

1.7.2 $z > 1$ support for fragmentation functions?

(Michelangelo) but this is already written up for the LHC report

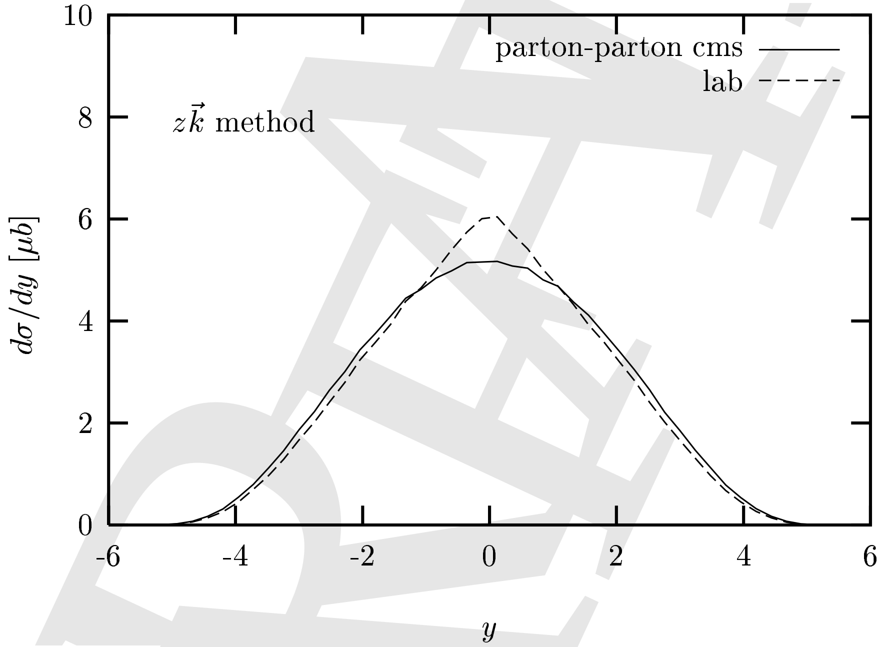

Figure 1.34:
Commutativity of boosting and fragmenting for rapidity (y) distribution.

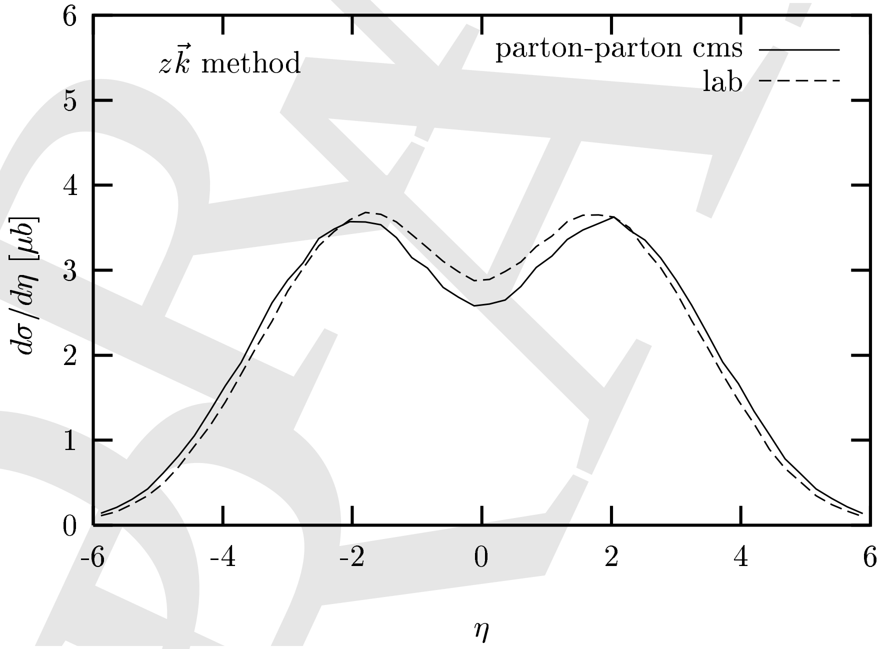

Figure 1.35:
Commutativity of boosting and fragmenting for pseudorapidity (η) distribution.

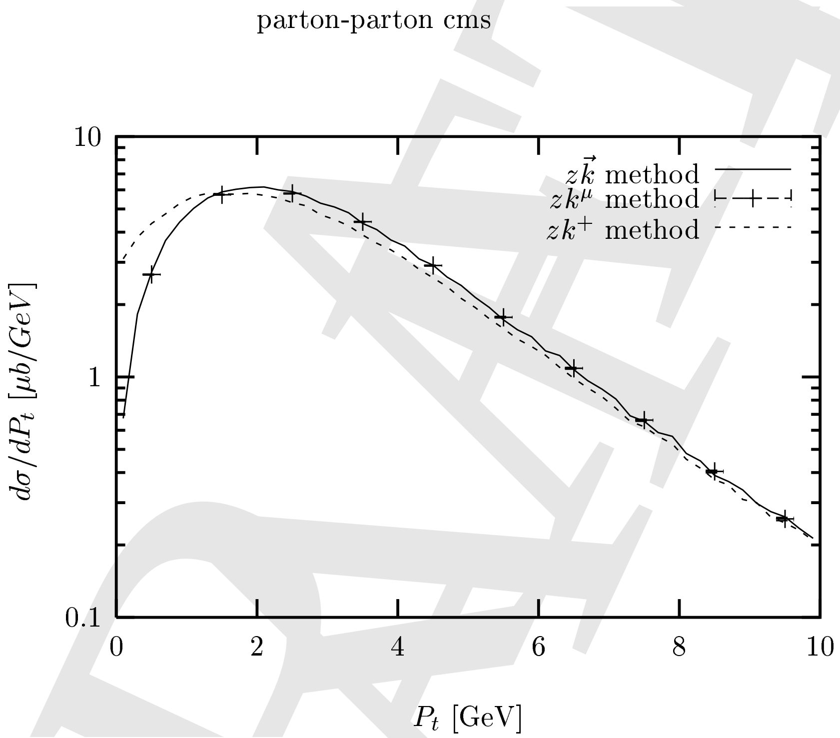

Figure 1.36:
Effect of fragmentation for different momentum components for P_T distribution.

acceptance	$\sigma[\mu b]$ lab.	parton cms $\sigma[\mu b]$
no cuts	26.24	26.24
$p_T > 0.5, \lvert\eta\rvert < 1.5$	9.66	8.87
$p_T > 5, \lvert\eta\rvert < 1.5$	2.58	2.53

Table 1.8: Interplay of boosting ambiguity with acceptance cuts.

1.8 Experimental impact

We shall try to assess to what extent and accurate knowledge of fragmentation issues is relevant for B-physics studies at the Tevatron. [Tagging rates?].

Also, SLD plots [Scott?].

References

[1] P. Nason, S. Dawson and R. K. Ellis, Nucl. Phys. B303, 607 (1988).

[2] W. Beenakker, H. Kuijf, W. L. van Neerven and J. Smith, Phys. Rev. **D40**, 54 (1989).

[3] P. Nason, S. Dawson and R. K. Ellis, Nucl. Phys. **B327**, 49 (1989).

[4] W. Beenakker, W. L. van Neerven, R. Meng, G. A. Schuler and J. Smith, Nucl. Phys. **B351**, 507 (1991).

[5] M. L. Mangano, P. Nason and G. Ridolfi, Nucl. Phys. **B373**, 295 (1992).

[6] R. K. Ellis and D. A. Ross, Nucl. Phys. **B345**, 79 (1990).

[7] S. Catani, M. Ciafaloni and F. Hautmann, Nucl. Phys. **B366**, 135 (1991).

[8] S. Catani, M. Ciafaloni and F. Hautmann, Phys. Lett. **B242**, 97 (1990).

[9] J. C. Collins and R. K. Ellis, Nucl. Phys. **B360**, 3 (1991).

[10] S. P. Baranov and M. Smizanska, Phys. Rev. **D62**, 014012 (2000).

[11] P. Nason, S. Dawson and R. K. Ellis, Nucl. Phys. B327, 49 (1989).

[12] S. Frixione and M. L. Mangano, Nucl. Phys. B483, 321 (1997) [hep-ph/9605270].

[13] DØ Collaboration, S. Abachi *et al.*, Phys. Rev. Lett. 74, 3548 (1995).

[14] DØ Collaboration, FERMILAB PUB-99/144-E and hep-ex/9905024.

[15] S.Frixione, M.Mangano, Nucl.Phys.B483, 321(1997).

[16] CDF Collaboration, F. Abe *et al.* Phys. Rev. D61, 32001,(2000).

[17] CDF Collaboration, F. Abe *et al.* Phys. Rev. D53, 1051,(1996).

[18] M. Mangano, P. Nason, and G. Ridolfi, Nucl. Phys. B373, 295 (1992).

[19] CDF Collaboration, F. Abe *et al.* Phys.Rev.Lett. 75, 1451,(1995).

[20] G. T. Bodwin, E. Braaten and G. P. Lepage, Phys. Rev. D51, 1125 (1995) [hep-ph/9407339]; erratum Phys. Rev. D55, 5853 (1997).

[21] For recent work on NRQCD, see M. E. Luke, A. V. Manohar and I. Z. Rothstein, Phys. Rev. D61, 074025 (2000) [hep-ph/9910209], and references therein.

[22] G. P. Lepage, L. Magnea, C. Nakhleh, U. Magnea and K. Hornbostel, Phys. Rev. D46, 4052 (1992) [hep-lat/9205007].

[23] P. Cho and A. K. Leibovich, Phys. Rev. D53, 6203 (1996) [hep-ph/9511315]; Phys. Rev. D53, 150 (1996) [hep-ph/9505329].

[24] A. Petrelli, hep-ph/9910274.

[25] E. Braaten, S. Fleming and A. K. Leibovich, work in progress.

[26] F. Abe et al., Phys. Rev. Lett. 75, 4358 (1995).

[27] J. L. Domenech and M. A. Sanchis-Lozano, Phys. Lett. B476, 65 (2000) [hep-ph/9911332].

[28] F. Abe *et al.*Phys. Rev. Lett. **79**,572(1997).

[29] F. Abe *et al.*Phys. Rev. Lett. **79**,578(1997).

[30] E. Braaten, M.A. Doncheski, S. Fleming and M.L. Mangano, Phys. Lett. **B 333**,548(1994); M. Cacciari and M. Greco, Rev. Lett. **73**,1586(1994); D.P. Roy and K. Sridhar Phys. Lett. **B 339**,141(1994).

[31] E. Braaten and S. Flemimg,Phys. Rev. Lett. **74**,3327(1995); M. Cacciari, M. Greco, M.L. Mangano and A. Petrelli, Phys. Lett. **B 356**,553(1995); P. Cho and A.K. Leibovich, Phys. ReV. D **53**,150(1996); P. Cho and A. K. Leibovich, Phys. ReV. D **53**,6203(1996).

[32] P. Cho and M. Wise, Phys. Lett. **B 346**,129(1995).

[33] T. Affolder *et al.*FERMILAB-PUB-00-90-E,Apr.,2000. Submitted to Phys. Rev. Lett. (2000).

[34] M. Beneke and M. Kramer, Phys. ReV. D **55**,5269(1997).

[35] E. Braaten, B. Kniehl and J. Lee, hep-ph/9911436.

[36] V. V. Kiselev, A. E. Kovalsky and A. K. Likhoded, hep-ph/0002127.

[37] A. K. Likhoded and A. I. Onishchenko, hep-ph/9912425.

[38] V. V. Kiselev, A. K. Likhoded and A. I. Onishchenko, hep-ph/9901224.

[39] V. V. Kiselev, A. K. Likhoded and A. I. Onishchenko, Phys. Rev. D60, 014007 (1999) [hep-ph/9807354].

[40] A. K. Likhoded and A. I. Onishchenko, hep-ph/9912425.

[41] J.D. Bjorken, 'Is the *ccc* a new deal for baryon spectroscopy', Fermilab-Conf-85/69.

[42] J.D. Bjorken, 'Estimate of Decay Branching ratios for hadrons containing Charm and Bottom quarks', unpublished Fermilab report (1986), (http://www-theory.fnal.gov/people/ellis/Bphysics/bjorken.PDF).

[43] J. Richard, hep-ph/9407224.

[44] B. Guberina, B. Melic and H. Stefancic, hep-ph/9911241.

[45] CDF Collaboration, F. Abe *et al.*, Phys. Rev. Lett. 81, 2432 (1998); and Phys. Rev. D58, 112004 (1998).

[46] S.S. Gershtein, V.V. Kiselev, A.K. Likhoded, A.V. Tkabladze, A.V. Berezhnoi, A.I. Onishchenko (Serpukhov, IHEP), Theoretical Status of the B_c Meson, presented at 4th International Workshop on Progress in Heavy Quark Physics, Rostock, Germany, 20-22 Sept. 1997, e-Print Archive: hep-ph/9803433.

[47] The OPAL Collab., K. Ackerstaff *et al.*, Phys. Lett. B420, 157 (1998);
The ALEPH Collab., R. Barate *et al.*, Phys. Lett. B402, 213 (1997);
The DELPHI Collab., P. Abreu *et al.*, Phys. Lett. B398, 207 (1997).

[48] V.V. Kiselev, A.E. Kovalsky, A.K. Likhoded (Serpukhov, IHEP) B_c Decays and lifetime in QCD Sum Rules, Feb 2000, e-Print Archive: hep-ph/0002127;
V.V. Kiselev, A.A. Likhoded (Serpukhov, IHEP), A.I. Onishchenko (Moscow, ITEP), Nucl. Phys. B569, 473 (2000);
A. Abd El-Hady, J.H. Munoz, J.P. Vary, Semileptonic and Nonleptonic B_c Decays, ISU-NP-99-08, IITAP-99-010, Sept. 1999., e-Print Archive: hep-ph/9909406; Chao-Hsi Chang, Yu-Qi Chen, Phys. Rev. D49 3399 (1994).

[49] P. Avery *et al.*, MCFAST: A Fast Simulation Package for Detector Design Studies, FERMILAB-CONF-97-151, June 1997, to be published in the proceedings of Computing in High-energy Physics (CHEP 97), Berlin, Germany, 7-11 Apr. 1997.

[50] P. Grannis and A. Lucotte, Extending the sensitivity to $\sin 2\beta$ in the $B^0/\bar{B}^0$ system using a low p_t $J/\psi \rightarrow e^+e^-$ trigger at DØ for Run II, DØ Note 3596, 10 Feb. 1999.

[51] F. Abe et al., CDF Collaboration, Phys. Rev. Lett. 81, 2432 (1998), Phys. Rev. D58, 112004 (1998).

[52] A.V. Berezhnoy, A.K. Likhoded, M.V. Shevlyagin, Yad. Fiz. 58, 730 (1995);
A.V. Berezhnoy, A.K. Likhoded, O.P. Yushenko, Yad. Fiz. 59, 742 (1996);
C.-H. Chang et al., Phys. Lett. B364, 78 (1995);
K. Kolodziej, A. Leike, R. Rückl, Phys. Lett. B355, 337 (1995);
A.V. Berezhnoy, V.V. Kiselev, A.K. Likhoded, Z.Phys. A356, 79 (1996).

[53] R.Akers et al., Z.Phys. C67 (1995) 27;
R.Akers et al., Phys. Lett. B353 (1995) 545.

[54] S.S. Gerstein et al., Heavy Ion Phys. 9 (1999) 133-144, [hep-ph/9811212].

[55] V.V. Kiselev, A.K. Likhoded, A.I. Onishchenko Phys. Rev. D60(1999), [hep-ph/9807354];
V.V. Kiselev, A.K. Likhoded, A.I. Onishchenko, [hep-ph/9901224];
A.K. Likhoded, A.I.Onishchenko [hep-ph/9912425]

[56] Onishchenko A.I., private communication;
Xin-Heng Guo, Hong-Ying Jin, Xue-Qian Li, Phys. Rev. D58 (1998), 114007, [hep-ph/9805301].

[57] J.D.Bjorken, draft report 07/22/86 (1986) [unpublished].

[58] F. Abe et al., CDF Collaboration, Phys. Rev. Lett. 81, 2432 (1998), Phys. Rev. D58, 112004 (1998).

[59] M.Neubert, Phys. Rep., 245, 259 (1994).

[60] G.T.Bodwin, E.Braaten, G.P.Lepage, Phys. Rev. D51, 1125 (1995);
T.Mannel, G.A.Schuller, Z. Phys. C67, 159 (1995).

[61] M.Lusignoli, M.Masetti, Z. Phys. C51, 549 (1991);
V.V.Kiselev, Mod. Phys. Lett. A10, 1049 (1995);
V.V.Kiselev, Int. J. Mod. Phys. A9, 4987 (1994);
V.V.Kiselev, A.K.Likhoded, A.V.Tkabladze, Yad. Fiz. 56, 128 (1993);
V.V.Kiselev, A.V.Tkabladze, Yad. Fiz. 48, 536 (1988);
G.R.Jibuti, Sh.M.Esakia, Yad. Fiz. 50, 1065 (1989), Yad. Fiz. 51, 1681 (1990);
C.-H.Chang, Y.-Q.Chen, Phys. Rev. D49, 3399 (1994);
D.Scora, N.Isgur, Phys.Rev. D52, 2783 (1995);
A.Yu.Anisimov, I.M.Narodetskii, C.Semay, B.Silvestre–Bra, Phys.Lett. B452, 129 (1999) [hep-ph/9812514];
A.Yu.Anisimov, P.Yu.Kulikov, I.M.Narodetsky, K.A.Ter-Martirosian, Phys.Atom.Nucl. 62, 1739 (1999), Yad.Fiz. 62, 1868 (1999), [hep-ph/9809249].

[62] I.Bigi, Phys. Lett. B371, 105 (1996);
M.Beneke, G.Buchalla, Phys. Rev. D53, 4991 (1996);
A.I.Onishchenko, [hep-ph/9912424].

[63] P.Colangelo, G.Nardulli, N.Paver, Z.Phys. C57, 43 (1993);
E.Bagan et al., Z. Phys. C64, 57 (1994).

[64] V.V.Kiselev, A.V.Tkabladze, Phys.Rev. D48, 5208 (1993).

[65] V.V.Kiselev, A.K.Likhoded, O.A.Onishchenko, DESY 99-053 (1999), hep-ph/9905359 [to appear in Nucl. Phys. B]. V.V.Kiselev, A.K.Likhoded, A.E.Kovalsky, hep-ph/0002127 (2000).

[66] E.Jenkins, M.Luke, A.V.Manohar, and M.J.Savage, Nucl. Phys. B390, 463 (1993).

[67] G.Chiladze, A.F.Falk, A.A.Petrov, Phys.Rev. D60, 034011 (1999);
C.H.Chang, J.P.Cheng, C.D.Lü, Phys.Lett. B425, 166 (1998);
T.M.Aliev, M.Savci, Phys.Lett. B434, 358 (1998), J.Phys. G25, 1205 (1999);
P.Colangelo, F.De Fazio, Mod.Phys.Lett. A33, 2303 (1999).

[68] S.S.Gershtein et al., preprint IHEP 98-22 (1998) [hep-ph/9803433];
V.V.Kiselev, Phys.Lett. B372, 326 (1996), hep-ph/9605451.

[69] M.Dugan and B.Grinstein, Phys. Lett. B255, 583 (1991);
M.A.Shifman, Nucl. Phys. B388, 346 (1992);
B.Blok, M.Shifman, Nucl. Phys. B389, 534 (1993).

[70] O.N.Pakhomova, V.A.Saleev, hep-ph/9911313 (1999).

[71] D.Du, X.Li, Y.Yang, Phys.Lett. B380, 193 (1996);
S.Fajfer, D.Prelovsek, P.Singer, Phys.Rev. D59, 114003 (1999);
T.M.Aliev, M.Savci, hep-ph/9908203 (1999).

[72] M.Masetti, Phys.Lett. B286, 160 (1992);
Y.S.Dai, D.S.Du, Eur.Phys.J. C9, 557 (1999).

[73] C.Quigg, in Proc of the Workshop on B Physics at Hadron Accelerators, Snowmass, Colorado, 1993, edts. P.McBride and C.S.Mishra [Fermilab, Batavia (1994)].

[74] J. Binnewies, B. A. Kniehl, and G. Kramer, Z. Phys. **C65**, 471 (1995), hep-ph/9407347.

[75] C. Peterson, D. Schlatter, I. Schmitt, and P. Zerwas, Phys. Rev. **D27**, 105 (1983).

[76] B. Mele and P. Nason, Nucl. Phys. **B361**, 626 (1991).

[77] P. Nason *et al.*, (1999), hep-ph/0003142.

[78] G. Altarelli and G. Parisi, Nucl. Phys. **B126**, 298 (1977).

[79] V. N. Gribov and L. N. Lipatov, Yad. Fiz. **15**, 781 (1972).

[80] Y. L. Dokshitzer, Sov. Phys. JETP **46**, 641 (1977).

[81] E. Braaten, K. Cheung, S. Fleming, and T. C. Yuan, Phys. Rev. **D51**, 4819 (1995), hep-ph/9409316.

[82] R. L. Jaffe and L. Randall, Nucl. Phys. **B412**, 79 (1994), hep-ph/9306201.

[83] P. Nason and C. Oleari, Nucl. Phys. **B521**, 237 (1998), hep-ph/9709360.

[84] G. Rodrigo, M. Bilenky, and A. Santamaria, Nucl. Phys. **B554**, 257 (1999), hep-ph/9905276.

[85] W. Bernreuther, A. Brandenburg, and P. Uwer, Phys. Rev. Lett. **79**, 189 (1997), hep-ph/9703305.

[86] P. Nason and C. Oleari, (1999), hep-ph/9903541.

[87] M. Cacciari and M. Greco, Nucl. Phys. **B421**, 530 (1994), hep-ph/9311260.

[88] M. Cacciari, M. Greco, and P. Nason, JHEP **05**, 007 (1998), hep-ph/9803400.

[89] F. I. Olness, R. J. Scalise, and W.-K. Tung, Phys. Rev. **D59**, 014506 (1999), hep-ph/9712494.

[90] M. Cacciari and M. Greco, Z. Phys. **C69**, 459 (1996), hep-ph/9505419.

[91] M. Cacciari *et al.*, Nucl. Phys. **B466**, 173 (1996), hep-ph/9512246.

[92] SLD, K. Abe *et al.*, Phys. Rev. Lett. **84**, 4300 (2000), hep-ex/9912058.

[93] J. C. Collins and D. E. Soper, Nucl. Phys. **B194**, 445 (1982).

[94] E. Norrbin and T. Sjostrand, Phys. Lett. **B442**, 407 (1998), hep-ph/9809266.

[95] E. Norrbin, (1999), hep-ph/9909437.